Efficient structural reliability analysis based on adaptive Bayesian support vector regression

Jinsheng Wang[a], Chenfeng Li[b,c], Yongle Li[a], Ahsan Kareem[d] and Guoji Xu[a,*]

[a] Department of Bridge Engineering, Southwest Jiaotong University, Chengdu, 610031, China.
[b] Zienkiewicz Centre for Computational Engineering, College of Engineering, Swansea University, Swansea, SA1 8EN, U.K.
[c] Energy Safety Research Institute, College of Engineering, Swansea University, Swansea, SA1 8EN, U.K.
[d] Department of Civil and Environmental Engineering and Earth Sciences, University of Notre Dame, Notre Dame, IN 46556, USA.

ARTICLE INFO

Keywords:
Structural reliability analysis
Adaptive surrogate models
Support vector regression
Bayesian inference
Learning function

ABSTRACT

To alleviate the computational burden for structural reliability analysis involving complex numerical models, many adaptive algorithms based on surrogate models have been developed. Among the various surrogate models, the support vector machine for regression (SVR) which is derived from statistical learning theory has revealed superior performance to handle nonlinear problems and avoid over fitting with excellent generalization ability. Therefore, to take the advantages of the desirable properties of SVR, an Adaptive algorithm based on the Bayesian SVR model (ABSVR) is proposed in this study. In ABSVR, a new learning function is devised for effective selection of informative sample points following the idea of the penalty function method in optimization. To avoid adding redundant samples that locate too close to the existing ones, a distance constraint term is added to the learning function. Besides, an adaptive sampling region scheme is employed to filter out samples with weak probability density to further enhance the efficiency of the proposed algorithm. Moreover, a hybrid stopping criterion based on error-based stopping criterion using the bootstrap confidence estimation is developed to terminate the active learning process, ensuring that the learning algorithm stops at an appropriate stage. The proposed ABSVR is easy to implement since no embedded optimization algorithm nor iso-probabilistic transformation is required. The performance of ABSVR is tested on six numerical examples featuring different complexity, and the results demonstrate the superior performance of ABSVR for structural reliability analysis both in terms of accuracy and efficiency.

1. Introduction

It is well recognized that the presence of uncertainties in practical engineering problems significantly affects the performance of structural systems, and uncertainty quantification with due consideration of these randomnesses are indispensable to the safety assessment, optimal design and serviceability maintenance of structures [1, 2]. Hence, structural reliability theory which gives a rational treatment and provides a quantitative evaluation of uncertainties has gained increasing attention in recent years. Structural reliability analysis aims to determine the probability of failure of a structural system with respect to some performance criterion in the presence of various uncertainties. Typically, the fundamental problem of structural reliability analysis can be mathematically defined as a multi-dimensional integral:

$$P_f = \text{Prob}[G(\boldsymbol{x}) \leq 0] = \int_{\Omega_f} f_{\boldsymbol{X}}(\boldsymbol{x}) d\boldsymbol{x} = \int_{\mathbb{R}^n} I_F(\boldsymbol{x}) f_{\boldsymbol{X}}(\boldsymbol{x}) d\boldsymbol{x} \tag{1}$$

where $\boldsymbol{x} = \left[x_1, x_2, ..., x_n\right]^T$ is a random vector with joint probability density function (PDF) $f_{\boldsymbol{X}}(\boldsymbol{x})$, representing the uncertainties arise from loading conditions, material properties, environmental factors, etc.; $G(\boldsymbol{x})$ is the limit state

*Corresponding author
jinshengwangrjc@swjtu.edu.cn (J. Wang); c.f.li@swansea.ac.uk (C. Li); lele@swjtu.edu.cn (Y. Li); kareem@nd.edu (A. Kareem); guoji.xu@swjtu.edu.cn (G. Xu)

function (LSF) defined in terms of $\boldsymbol{x}$, i.e. $G(\boldsymbol{x}) : \chi \subseteq \mathbb{R}^n \to \mathbb{R}, \boldsymbol{x} \mapsto g(\boldsymbol{x})$; Ω_f is the failure domain defined such that $\Omega_f = \{\boldsymbol{x} \in \chi : G(\boldsymbol{x}) \leq 0\}$, with its complementary set $\Omega_s = \{\boldsymbol{x} \in \chi : G(\boldsymbol{x}) > 0\}$ denoting the safe domain and $\Omega_0 = \{\boldsymbol{x} \in \chi : G(\boldsymbol{x}) = 0\}$ representing the limit state surface (LSS); and $I_F(\boldsymbol{x})$ is the indicator function defined as:

$$I_F(\boldsymbol{x}) = I_{\Omega_f}(\boldsymbol{x}) = \begin{cases} 1 & \boldsymbol{x} \in \Omega_f \\ 0 & \boldsymbol{x} \in \Omega_s \end{cases} \tag{2}$$

The definition of failure probability in Eq. (1) is simple, but its calculation by direct integration is often intractable because the dimensionality of the integral is generally high and the LSS is of complicated geometry, especially for complex physical problems. The challenge of accurately computing this integral has led to the development of various approximation methods, among which the Monte Carlo simulation (MCS) is one of the most commonly used methods because it is simple to implement and insensitive to the problem's specific nature. The MCS approach generates sample points using the distribution function associated with each random variable to estimate the failure probability, which is approximated as the ratio of failure realizations to the total number of evaluations:

$$P_f \approx \widehat{P}_f^{\mathrm{MCS}} = \frac{1}{N} \sum_{i=1}^{N} I_F(\boldsymbol{x}^i) \tag{3}$$

where $\widehat{P}_f^{\mathrm{MCS}}$ is the failure probability estimator of MCS, and $\left\{\boldsymbol{x}^{(i)}, i = 1, \ldots, N\right\}$ is the Monte Carlo population with a sample size of N. This estimator is asymptotically unbiased according to the central limit theorem, and its coefficient of variation is:

$$\delta_{\mathrm{MCS}} = \sqrt{\frac{1 - P_f}{N P_f}} \tag{4}$$

Thus, to ensure a small variation of the failure probability estimation, the required number of samples can be prohibitively high, i.e. the convergence rate is low $\left(\propto N^{-1/2}\right)$, especially for rare failure events. Numerous methods have been developed to reduce the computational cost of reliability analysis, and they can be broadly classified into five different groups, namely the approximate analytical methods [3, 4], the advanced simulation methods [5, 6], the moment methods [7, 8], the probability density evaluation methods [9, 10] and the surrogate-based methods [11–13]. Although the advanced simulation methods, such as importance sampling [14, 15], directional simulation [16, 17], line sampling [18], hierarchical failure clustering (HFC) [19] and subset simulation [20, 21]), can greatly enhance the efficiency of MCS, the computational burden is still excessive for practical engineering problems. As an efficient alternative to the simulation methods, the analytical methods such as first-order reliability method (FORM) [22, 23] and second-order reliability method (SORM) [24, 25] are well-known for its simplicity and efficiency. In these methods, the performance function is usually approximated by a low-order (linear or quadratic) Talyor series expansion at the most probable point (MPP), where the isoprobabilistic transformation techniques are usually employed to transform the random variables from the physical space to the standard normal space [26, 27], as illustrated in Fig. 1. Although they can provide reasonably accurate results with remarkable efficiency for some specific problems, the iterative MPP

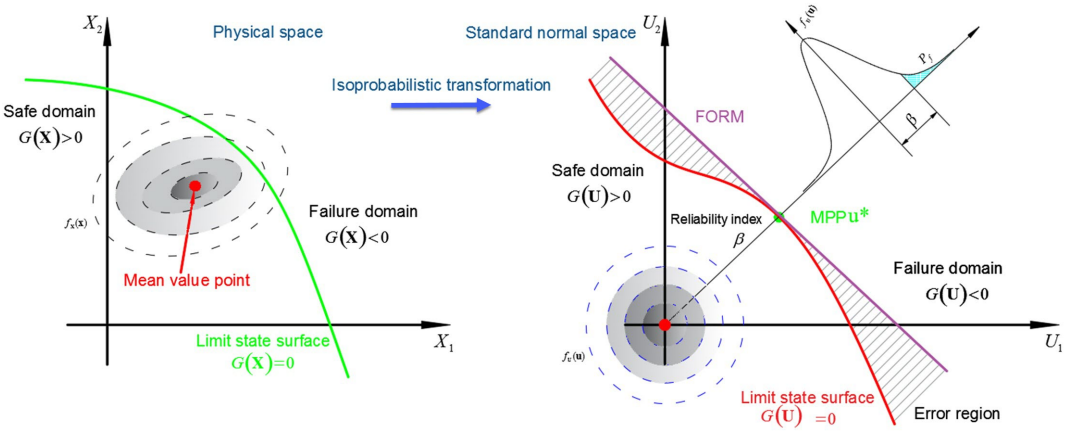

Figure 1: Isoprobabilistic transformation from physical space to standard normal space (adapted from [28].)

searching process may encounter non-convergence issues and the accuracy of the generated results cannot be guaranteed for problems with multiple MPPs and/or with highly nonlinear LSF. In this regard, the surrogate-based methods, which can reach a good trade-off between efficiency and accuracy, are of particular interest in this paper.

The key idea of surrogate-based methods is to construct an easy-to-evaluate mathematical model to replace the original complex LSF, through which many more simulation runs can be readily afforded [29]. Some of the representative surrogate modeling techniques include the response surface method (RSM) [30, 31], the polynomial chaos expansion (PCE) [32, 33] , the Kriging method [34, 35], the radial basis function (RBF) [36, 37], the support vector machine (SVM) (formulated in terms of classification (SVM) [38] or regression (SVR)) [39, 40], the artificial neural networks (ANN) [41–43] and more recently, the ensemble of surrogates [44], among others. A crucial issue for the construction of these surrogate models is the selection of an appropriate design of experiment (DoE), i.e. input-output training pairs. In general, there are two strategies for the DoE selection, namely the one-shot sampling schemes and the sequential sampling methods. The traditional one-shot sampling methods try to generate space-filling samples over the entire random space with predefined sample size. In the context of structural reliability analysis, however, only regions near the LSS are of great interest and the appropriate number of samples is hard to determine *a priori* as too large or too small the sample size will both jeopardize the performance of surrogate-based methods. Therefore, various adaptive sampling schemes capable of exploiting the information contained in the constructed surrogate model have been developed to enrich the DoE in an iterative manner [37, 45, 46]. Reliability analysis methods empowered with adaptive sampling schemes are known as the active learning methods, where a preliminary surrogate model is established based on the initial DoE and then updated by sequentially enriching the DoE according to some judiciously selected learning functions. The general procedure of surrogate-based active learning method for reliability analysis is illustrated in Fig. 2. By doing so, the efficiency of structural reliability analysis can be significantly improved without compromising the accuracy.

Considering the superior performance of surrogate-based active learning methods, the development of effective learning algorithms is an active research topic in structural reliability community. Bichon et al. [47] proposed an Efficient Global Reliability Analysis (EGRA) method, in which a learning function known as Expected Feasibility

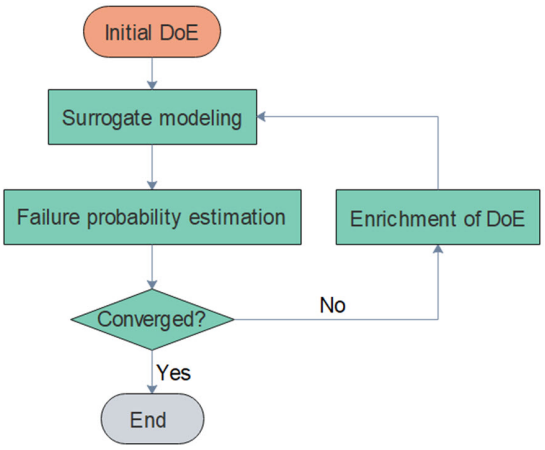

Figure 2: The general procedure of surrogate-based active learning method for reliability analysis.

Function (EFF) is applied to select the new samples for the enrichment of DoE. This learning function indicates how well a point is expected to locate on the LSS, i.e. $G(\boldsymbol{x}) = 0$. The accuracy and efficiency of this method are demonstrated through numerical examples, yet its global approximation property may introduce redundant points with weak probability densities. To address this issue, an active learning method known as AK-MCS that combines Kriging with crude MCS was developed by Echard et al. [48]. In AK-MCS, a large number of Monte Carlo populations are evaluated on the learning function U, and the one that minimizes U is selected as the best next point to be added to the DoE. This learning process enables the selection of samples with large probability density and assigns more weights to the points close to the LSS. An active SVR-based method was presented in [49], where an adaptive algorithm is proposed for selecting samples close to the LSS by rotating the experimental design according to the directions of the gradient of the established SVR model. To effectively generate samples in the most likely failure regions, the Markov chain simulation is employed in [50], where the SVR model is iteratively refined by adding new Markov chain samples. Thanks to these pioneering works, new adaptive algorithms are emerging to further improve the computational accuracy and efficiency of structural reliability analysis, which can be summarized into the following aspects:

- **New learning functions:** More effective learning functions are developed to select sample points in the vicinity of LSS (e.g. the learning function H based on information entropy theory [51], the learning function REIF and FNEIF based on folded normal distribution [52, 53]), to account for dependencies between the Kriging predictions (e.g. [54, 55]), to avoid clustering of the generated samples (e.g. [40, 56]), and to consider the joint PDF of random variables (e.g. the least improvement function(LIF) [57], the learning function REIF2 [52] and the active weight learning function (U_{AWL}) [58]).

- **Rare failure events:** Integration methods are developed to deal with problems of small failure probability, and they include importance sampling (AK-IS) [59–62], line sampling [63], subset simulation (e.g. AK-SS [64, 65], [2] SMART [66] and ASVR [67]), and spherical decomposition-MCS [68, 69], among others.

- **Effective sampling regions:** Sampling regions are better defined to enhance the computational efficiency, and

they include the adaptive trust region method [70], the adaptive sampling region method [71, 72], and the probability-adaptive Kriging method based on sampling in n-Ball (PAK-B^n) [73].

- **New stopping criteria:** New stopping criteria are developed for more accurate termination of the learning process to avoid premature of the algorithm or unnecessary calls to the performance functions, and the include the error-based stopping criterion (ESC) [74, 75] and its improvement based on bootstrap confidence estimation (BCE) [76].

- **Extended applications:** Adaptive algorithms are extended to solve system reliability problems (e.g. EGRA [77], AK-SYS [78], CSF-ALK [79], EEK-SYS [80], and [81]), to enhance the computational efficiency of reliability based design optimization (RBDO) (e.g. [82, 83]), and to efficiently deal with problems of imprecise probability models (e.g. [84, 85]).

However, it is noted that most of the aforementioned active learning methods are developed based on the Kriging model, where the error at unknown points can be empirically measured by the Kriging variance. Thus, the use of these learning algorithms to other surrogate models is not directly applicable unless additional effort such as bootstrap resampling strategy [86] or k fold cross-validation [87] is employed to get the prediction variance, which is a cumbersome process. To address this issue, several studies have been devoted to getting the model variance in a more effective way, among which the recently proposed Bayesian inference framework has shown promising potential [88, 89]. The Bayesian compressed sensing (BCS) technique is incorporated with a parameterized prior for the establishment of sparse PCE in [88], whereas Bayesian SVR models are developed based on different loss functions using Bayesian inference theory in [89, 90]. Similar to the Kriging method, the Bayesian sparse PCE and Bayesian SVR are capable of providing probabilistic prediction at a new point under the Gaussian process assumption. Therefore, the ideas underlying Kriging-based active learning algorithms can readily be adapted to these Bayesian induced surrogate models [91, 92].

Unlike models such as ANN and PCE which apply the principle of empirical risk minimization to mimic a true model, the SVR (stems from SVM for regression) is developed in the field of statistical learning theory and has revealed superior performance to handle nonlinear problems and avoid overfitting with good generalization ability. In this regard, the adaptive algorithm based on Bayesian SVR is expected to be well-suited for structural reliability analysis. In this paper, a novel Adaptive Bayesian SVR method (ABSVR) that combines with sampling region scheme and hybrid stopping criterion is proposed for efficient reliability analysis with high accuracy. Following the idea of penalty function method in optimization, a new sampling-based learning function (SLF) is devised for effective selection of informative sample points, e.g. points close to the LSS in critical regions with significant contribution to the failure probability. To avoid adding redundant samples clustering with the existing ones, a distance constraint term is added to the learning function. Besides, the adaptive sampling region scheme [71] originally developed for Kriging-based approach is adapted here to filter out sample points in regions with weak probability density, in that the samples in these regions have a negligible effect on the failure probability evaluation. In this way, the computational efficiency of ABSVR can be enhanced by using a set of important samples. Moreover, a hybrid stopping criterion based on the bootstrap confidence estimation (BCE) proposed in [76] is developed to terminate the active learning process,

ensuring that the learning algorithm stops at an appropriate stage. The proposed ABSVR is easy to implement since no embedded optimization algorithm nor iso-probabilistic transformation is required.

The rest of this paper is organized as follows. The basic principle of Bayesian SVR models is introduced in § 2. The following section recalls two advanced schemes for adaptive algorithm, namely the adaptive sampling region scheme and the error-based stopping criterion. § 4 presents the detailed derivation of the new learning function, and the hybrid stopping criterion is proposed in § 5. The implementation procedure of the proposed ABSVR is summarized in § 6. The accuracy, efficiency and robustness of ABSVR are illustrated in § 7 using several numerical examples. Finally, concluding remarks are drawn in § 8.

2. Basic theory of Bayesian support vector regression

In this section, the basic theory of Bayesian support vector regression (BSVR) [89, 90, 92] is briefly recapped, with an emphasis on the BSVR models established with the square loss function (SLF) and the ε-insensitive square loss function (EISLF):

$$\ell_{\mathrm{SLF}}(\delta) = \frac{1}{2}\delta^2 \tag{5}$$

$$\ell_{\mathrm{EISLF}}(\delta) = \begin{cases} 0, & \text{if } |\delta| \le \varepsilon \\ \frac{1}{2}(|\delta| - \varepsilon)^2, & \text{otherwise} \end{cases} \tag{6}$$

where ε (with $\varepsilon > 0$) is an unknown parameter to be determined. It is noted that a soft insensitive loss function (SILF) is presented in [90] for the same purpose.

2.1. Bayesian inference framework

In regression problems, a set of paired samples, i.e. $\mathcal{D} = \left\{\left(\boldsymbol{x}_i, y_i\right) \mid i = 1, \ldots, N, \boldsymbol{x}_i \in \mathbb{R}^n, y_i \in \mathbb{R}\right\}$, are used as the training data for inferring the functional relation $h(\boldsymbol{x})$ such that:

$$y_i = h\left(\boldsymbol{x}_i\right) + \delta_i \quad i = 1, 2, \ldots, N \tag{7}$$

where $\boldsymbol{\delta} = \left[\delta_1, \delta_2, \cdots, \delta_N\right]^T$ are independent identically distributed random noises with the probability distribution $\mathcal{P}\left(\delta_i\right)$:

$$\mathcal{P}(\delta) = \frac{1}{\mathcal{Z}_\delta} \exp(-\eta \ell(\delta)) \tag{8}$$

where $\mathcal{Z}_\delta = \int \exp(-\eta \ell(\delta)) d\delta$, η is a constant value greater than zero and $\ell(\delta)$ is one of the loss functions defined in Eq. (6) and Eq. (5).

In the Bayesian framework, the regression model $h\left(\boldsymbol{x}_i\right)$ is assumed as a zero-mean stationary Gaussian process, with the covariance between two outputs defined as:

$$\mathrm{Cov}\left[h\left(\boldsymbol{x}_i\right), h\left(\boldsymbol{x}_j\right)\right] = k\left(\boldsymbol{x}_i, \boldsymbol{x}_j\right) = \prod_{k=1}^{n} \exp\left(-\theta_k \left(x_i^k - x_j^k\right)^2\right) \tag{9}$$

where $\boldsymbol{\theta} = \left[\theta_1, \theta_2, \cdots, \theta_n\right]^T$ are the corresponding hyper-parameters. Let $\boldsymbol{\chi}$ denote all hyper-parameters in the regression model and $\mathcal{H} = \left[h\left(\boldsymbol{x}_1\right), h\left(\boldsymbol{x}_2\right), \cdots, h\left(\boldsymbol{x}_N\right)\right]^T$. Then, given $\boldsymbol{\chi}$, the prior probability of $\mathcal{H}$ is a multivariate Gaussian distribution:

$$\mathcal{P}(\mathcal{H} \mid \boldsymbol{\chi}) = \frac{1}{\mathcal{Z}_{\mathcal{H}}} \exp\left(-\frac{1}{2}\mathcal{H}^T \mathcal{R}^{-1} \mathcal{H}\right) \tag{10}$$

where $\mathcal{R} \in \mathbb{R}^{N \times N}$ is the covariance matrix with the ijth element expressed as $\mathcal{R}_{ij} = \operatorname{Cov}\left[h\left(\boldsymbol{x}_i\right), h\left(\boldsymbol{x}_j\right)\right], i, j = 1, 2, \ldots, N$, and $\mathcal{Z}_{\mathcal{H}} = (2\pi)^{N/2}|\mathcal{R}|^{1/2}$. Given that the random noises $\boldsymbol{\delta} = \left[\delta_1, \delta_2, \cdots, \delta_N\right]^T$ are independent identically distributed, the likelihood function of the given data set $\mathcal{D}$ can be evaluated as [90]:

$$\mathcal{P}(\mathcal{D} \mid \mathcal{H}, \boldsymbol{\chi}) = \prod_{\mathrm{i}=1}^{N} \mathcal{P}\left(y_i - h\left(\boldsymbol{x}_i\right) \mid \boldsymbol{G}, \gamma\right) = \prod_{i=1}^{N} \mathcal{P}\left(\delta_i\right) \tag{11}$$

where the probability distribution $\mathcal{P}\left(\delta_i\right)$ of δ_i is given in Eq. (8). Substituting Eq. (10) and Eq. (11) into the Bayes' theorem $\mathcal{P}(\mathcal{H} \mid \mathcal{D}, \boldsymbol{\chi}) = \frac{\mathcal{P}(\mathcal{D}|\mathcal{H}, \boldsymbol{\chi})\mathcal{P}(\mathcal{H}|\boldsymbol{\chi})}{\mathcal{P}(\mathcal{D}|\boldsymbol{\chi})}$, the posterior probability $\mathcal{P}(\mathcal{H} \mid \mathcal{D}, \boldsymbol{\chi})$ of $\mathcal{H}$ can be derived as:

$$\mathcal{P}(\mathcal{H} \mid \mathcal{D}, \boldsymbol{\chi}) = \frac{1}{\mathcal{Z}} \exp\left(-\eta \sum_{i=1}^{N} \ell\left(y_i - h\left(\boldsymbol{x}_i\right)\right) - \frac{1}{2}\mathcal{H}^T \mathcal{R}^{-1} \mathcal{H}\right) \tag{12}$$

where $\mathcal{Z} = \int \exp(-S(\mathcal{H}))d\mathcal{H}$ with $S(\mathcal{H}) = \eta \sum_{i=1}^{N} \ell\left(y_i - h\left(\boldsymbol{x}_i\right)\right) + \frac{1}{2}\mathcal{H}^T \mathcal{R}^{-1} \mathcal{H}$. Thus, the maximum *a posteriori* estimate of $\mathcal{P}(\mathcal{H} \mid \mathcal{D}, \boldsymbol{\chi})$ is equivalent to the minimizer of the following optimization problem [89, 92]:

$$\min_{\mathcal{H}} S(\mathcal{H}) = \eta \sum_{i=1}^{N} \ell\left(y_i - h\left(\boldsymbol{x}_i\right)\right) + \frac{1}{2}\mathcal{H}^T \mathcal{R}^{-1} \mathcal{H} \tag{13}$$

2.2. Bayesian support vector regression

Introducing the square loss function defined in Eq. (5) into the optimization problem described in Eq. (13), the minimization problem is reformulated as [89]:

$$\min_{\mathcal{H}} \frac{1}{2}\mathcal{H}^T \mathcal{R}^{-1} \mathcal{H} + \frac{\eta}{2} \sum_{i=1}^{N} \zeta_i^2 \tag{14}$$

subject to

$$y_i = h\left(\boldsymbol{x}_i\right) + \zeta_i \tag{15}$$

The optimal solution of the above optimization problem is as:

$$\widehat{\mathcal{H}}_{\mathrm{SLF}} = \mathcal{R}(\mathcal{R} + \boldsymbol{I}/\eta)^{-1} \mathcal{Y} \tag{16}$$

where $\boldsymbol{I} \in \mathbb{R}^{N \times N}$ is an identity matrix, and $\mathcal{Y} = \left\{y_1, \cdots, y_N\right\}^{\mathrm{T}}$.

Similarly, using the ε-insensitive square loss function defined in Eq. (6), the optimization problem in Eq. (13) can be formulated as a constrained convex optimization problem by introducing slack variables $\boldsymbol{\xi} = \left(\xi_1, \ldots, \xi_N\right)$ and

$\boldsymbol{\xi}^* = \left(\xi_1^*, \ldots, \xi_N^*\right)$:

$$\min_{\mathcal{H}} \frac{1}{2}\mathcal{H}^T \mathcal{R}^{-1}\mathcal{H} + \frac{\eta}{2}\sum_{i=1}^{N}\left(\xi_i^2 + \xi_i^{*2}\right) \tag{17}$$

subject to

$$\begin{cases} y_i - h\left(\boldsymbol{x}_i\right) \leq \varepsilon + \xi_i & \text{for } i = 1, \ldots, N \\ h\left(\boldsymbol{x}_i\right) - y_i \leq \varepsilon + \xi_i^* & \text{for } i = 1, \ldots, N \\ \xi_i, \xi_i^* \geq 0 & \text{for } i = 1, \ldots, N \end{cases} \tag{18}$$

The optimal solution of the above optimization problem (Eq. (17) and Eq. (18)) can be facilitated in the context of Lagrange duality, which leads to the following regression function:

$$\widehat{\mathcal{H}}_{\text{EISLF}} = \mathcal{R}\left(\boldsymbol{\alpha} - \boldsymbol{\alpha}^*\right) \tag{19}$$

where $\boldsymbol{\alpha}^* = \left(\alpha_1^*, \cdots, \alpha_N^*\right)^{\mathrm{T}}, \boldsymbol{\alpha} = \left(\alpha_1, \cdots, \alpha_N\right)^{\mathrm{T}}$ are the Lagrangian multipliers, and support vectors are defined as the sample points with $\alpha_i - \alpha_i^* \neq 0$.

The remaining problem is to find the optimal values for the hyper-parameters in the support vector regression (SVR) model. In the Bayesian framework, the hyper-parameters can be obtained by solving the following maximization problem:

$$\max_{\chi} \mathcal{P}(\mathcal{D} \mid \chi) = \int \mathcal{P}(\mathcal{D} \mid \mathcal{H}, \chi)\mathcal{P}(\mathcal{H} \mid \chi)\boldsymbol{d}\mathcal{H} = \mathcal{Z}_{\mathcal{H}}^{-1}\mathcal{Z}_{\delta}^{-N}\int \exp(-S(\mathcal{H}))\boldsymbol{d}\mathcal{H} \tag{20}$$

For the SVR model established using the SLF $\ell_{\text{SLF}}(\delta)$, the maximization problem in Eq. (19)) can be transformed into the following minimization problem [89]:

$$\min_{\chi} -\ln(\mathcal{P}(\mathcal{D} \mid \chi)) = \eta\sum_{i=1}^{N}\ell_{\text{SLF}}\left(y_i - \widehat{h}\left(\boldsymbol{x}_i\right)\right) + \frac{1}{2}\boldsymbol{\beta}^T\mathcal{R}\boldsymbol{\beta} + \frac{1}{2}\ln|\boldsymbol{I} + \eta\mathcal{R}| + \frac{N}{2}\ln(\frac{2\pi}{\eta}) \tag{21}$$

where $\boldsymbol{\beta} = \left[\beta_1, \cdots, \beta_N\right]^{\mathrm{T}} = (\mathcal{R} + \boldsymbol{I}/\eta)^{-1}\mathcal{Y}$. Similarly, for the SVR model established using the EISLF $\ell_{\text{EISLF}}(\delta)$, with $S(\mathcal{H})$ approximated by a second order expansion, the maximization problem in Eq. (19)) can be reformulated as [89]:

$$\min_{\chi} -\ln(\mathcal{P}(\mathcal{D} \mid \chi)) = \eta\sum_{i=1}^{N}\ell_{\text{EISLF}}\left(y_i - \widehat{h}\left(\boldsymbol{x}_i\right)\right) + \frac{1}{2}\left(\boldsymbol{\alpha} - \boldsymbol{\alpha}^*\right)^T\mathcal{R}\left(\boldsymbol{\alpha} - \boldsymbol{\alpha}^*\right) + \frac{1}{2}\ln|\mathcal{L}| + N\ln(2\varepsilon + \sqrt{\frac{2\pi}{\eta}}) \tag{22}$$

where $\mathcal{L} = \mathbf{I} + \eta\boldsymbol{\Lambda}\mathcal{R}$, and $\boldsymbol{\Lambda}$ is a diagonal matrix with its entry equal to 1 for support vectors and zero otherwise.

2.3. Probabilistic prediction of BSVR

Under the Gaussian process assumption, the posterior distribution of $h(\boldsymbol{x})$ is Gaussian [89, 90]:

$$\mathcal{P}(h(\boldsymbol{x}) \mid \mathcal{D}) = N\left(\widehat{\mu}(\boldsymbol{x}), \widehat{\sigma}^2(\boldsymbol{x})\right) \tag{23}$$

where $\widehat{\mu}(\boldsymbol{x})$ and $\widehat{\sigma}^2(\boldsymbol{x})$ are the mean and variance of the BSVR model, respectively. For the SLF-based BSVR model, the $\widehat{\mu}_s(\boldsymbol{x})$ and $\widehat{\sigma}_s^2(\boldsymbol{x})$ can the obtained as:

$$\widehat{\mu}_s(\boldsymbol{x}) = \boldsymbol{k}(\boldsymbol{x}, \boldsymbol{X})(\mathcal{R} + \boldsymbol{I}/\eta)^{-1}\mathcal{Y} \tag{24}$$

$$\widehat{\sigma}_s^2(\boldsymbol{x}) = k(\boldsymbol{x}, \boldsymbol{x}) - \boldsymbol{k}(\boldsymbol{x}, \boldsymbol{X})(\mathcal{R} + \boldsymbol{I}/\eta)^{-1}\boldsymbol{k}(\boldsymbol{X}, \boldsymbol{x}) \tag{25}$$

where $\boldsymbol{X} = \left\{\boldsymbol{x}_1, \cdots, \boldsymbol{x}_N\right\}^{\mathrm{T}}$, and $\boldsymbol{k}(\boldsymbol{x}, \boldsymbol{X}) = \boldsymbol{k}(\boldsymbol{X}, \boldsymbol{x})^{\mathrm{T}} = \left[k\left(\boldsymbol{x}_1, \boldsymbol{x}\right), \cdots, k\left(\boldsymbol{x}_N, \boldsymbol{x}\right)\right]^{\mathrm{T}}$ is the covariance vector between $h(\boldsymbol{x})$ at a new point $\boldsymbol{x}$ and those in $\mathcal{H}$ evaluated at $\boldsymbol{X}$, which can be calculated from Eq. (9). For the EISLF-based BSVR model, the $\widehat{\mu}_e(\boldsymbol{x})$ and $\widehat{\sigma}_e^2(\boldsymbol{x})$ can the obtained as:

$$\widehat{\mu}_e(\boldsymbol{x}) = \boldsymbol{k}(\boldsymbol{x}, \boldsymbol{X})\mathcal{R}^{-1}\widehat{\mathcal{H}}_{\mathrm{EISLF}} = \sum_{j=1}^{m}\left(\alpha_j - \alpha_j^*\right)\boldsymbol{k}\left(\boldsymbol{x}, \boldsymbol{x}_j\right) \tag{26}$$

$$\widehat{\sigma}_e^2(\boldsymbol{x}) = k(\boldsymbol{x}, \boldsymbol{x}) - \boldsymbol{k}_m\left(\boldsymbol{x}, \boldsymbol{X}_m\right)\left(\mathcal{R}_m + \boldsymbol{I}_m/\eta\right)^{-1}\boldsymbol{k}_m\left(\boldsymbol{X}_m, \boldsymbol{x}\right) \tag{27}$$

where $\widehat{\mathcal{H}}_{\mathrm{EISLF}}$ is given in Eq. (19), $\boldsymbol{k}_m\left(\boldsymbol{x}, \boldsymbol{X}_m\right)$ and $\mathcal{R}_m$ are the subsets of $\boldsymbol{k}(\boldsymbol{x}, \boldsymbol{X})$ and $\mathcal{R}$, repectively, with their elements evaluated at the support vectors $\boldsymbol{X}_m$.

The BSVR models are established following the above procedures, and more information regarding the derivation of BSVR can be found in [89, 90, 92]. The probabilistic prediction parameters $\widehat{\mu}(\boldsymbol{x})$ and $\widehat{\sigma}^2(\boldsymbol{x})$ can now be employed to devise active learning algorithms for efficient reliability analysis based on the BSVR model, which is the main focus of this paper and will be explained in the following sections.

3. The advanced schemes for adaptive algorithm

The critical role of learning function in adaptive algorithms is well-recognised, while the influence of effective sampling regions for the selection of sample points and the error-based stopping criteria for the termination of the learning process did not draw too much attention until recently. Indeed, improper sampling scheme may introduce samples with weak probability densities that make barely any contribution to the failure probability, whereas inadequate selection of stopping criterion may lead to inaccurate estimation of the failure probability or results in high computational cost because of unnecessary calls to the performance function. Both can adversely affect the performance of an adaptive algorithm. To address these issues, several sampling region schemes (SRS) [71–73] and error-based stopping criteria (ESC) [74–76] have been proposed for effective reliability analysis. In this study, the sampling region scheme presented in [71] and the ESC using bootstrap confidence estimation (BCE) [76] will be integrated into the proposed method, namely the ABSVR.

3.1. Adaptive sampling region scheme

In the adaptive SRS, the region with the probability density larger than a threshold is progressively updated in the learning process, rather than fixing the sampling region in a predefined domain. The region of interest in this scheme

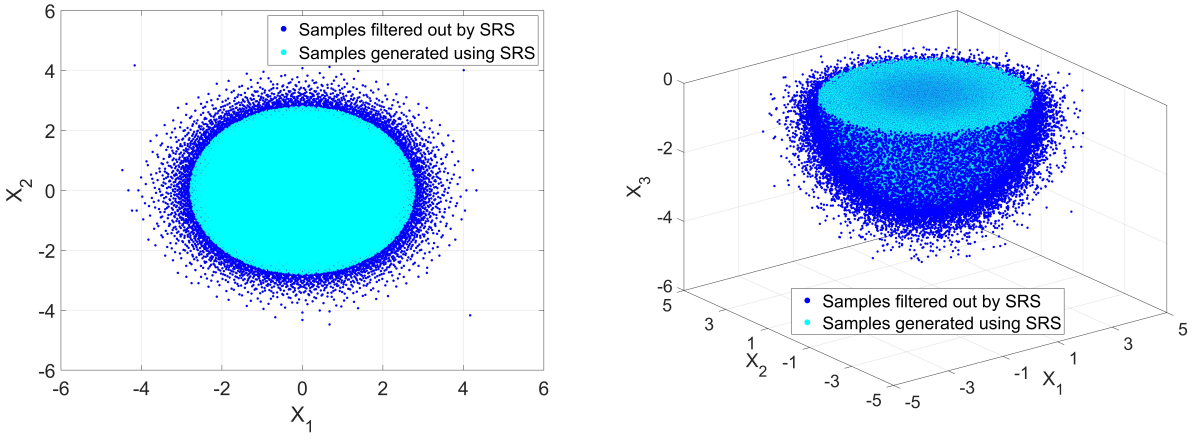

Figure 3: Schematic illustration of the SRS with $p_t^{(i)} = 0.1$ and $\alpha = 0.2$: (a) a 2D case; (b) a 3D case (only half of the ball is shown). (For interpretation of the references to color in this figure, please refer to the web version of this article.)

is given as [71]:

$$\hat{\Omega}_{(i)} = \left\{ \forall \boldsymbol{x} : f_{\boldsymbol{X}}(\boldsymbol{x}) > p_t^{(i)} \right\} \quad (i = 1, 2, \ldots) \tag{28}$$

where $p_t^{(i)}$ is the threshold value of the probability density in the i-th iteration, and can be determined according to the following equation:

$$P\left\{ f_{\boldsymbol{X}}(\boldsymbol{x}) < p_t^{(i)} \right\} = \alpha \hat{P}_f^{i-1} \tag{29}$$

where $P\left\{ f_{\boldsymbol{X}}(\boldsymbol{x}) < p_t^{(i)} \right\}$ denotes the probability of the joint PDF of the random variables being smaller than $p_t^{(i)}$, $\hat{P}_f^{i-1}$ is the failure probability estimated from the established BSVR model in the $(i-1)$-th iteration of the learning process, α is the coefficient used to control the size of the sampling region and can generally be selected from $[0.05, 0.2]$.

In each iteration, the threshold value $p_t^{(i)}$ can be obtained as the $(\alpha \hat{P}_f^{i-1})$-th percentile of the variable $\mathcal{F} = f_{\mathbf{X}}(\boldsymbol{x})$ by means of MCS. Once the sampling region as expressed in Eq. (28) is defined, the candidate samples for learning is generated in this region, thus those with small probability density will not be selected. In this way, the samples with negligible effects on the failure probability estimation will be filtered out, which can greatly enhance the efficiency of the learning algorithm. To facilitate a visual understanding of the idea underlying the SRS, two illustrative examples are given Fig. 3, where $p_t^{(i)}$ is assumed to be 0.1 and $\alpha = 0.2$. It is noted that the MCS population consists of the samples being filtered out by SRS (blue points) and the remaining ones in the inner region (cyan points). In the learning process, only the cyan points will be used as the candidate points to select the next best sample.

3.2. Error-based stopping criterion using BCE

Besides the SRS as described in the previous section, choosing the appropriate stopping criterion can also improve the efficiency of the adaptive algorithm. One of the most widely used stopping criteria is derived by setting a threshold value for the learning function [47, 48, 52]. However, they are often inadequate for the learning algorithm due to the lack of direct correspondence to the error of failure probability estimation, which is the parameter of particular

interest. This limitation may lead to inaccurate estimation of the failure probability or results in high computational burden because of unnecessary calls to the performance function. To effectively address this issue, an error-based stopping criterion (ESC) expressed in terms of the upper bound of the estimation error is proposed in [74, 75]. In this approach, the relative error ε_r of the predicted failure probability $\widehat{P}_f$ with respect to the reference result by MCS P_f^{MCS} is defined:

$$\varepsilon_r = \left| \frac{P_f^{\mathrm{MCS}} - \widehat{P}_f}{P_f^{\mathrm{MCS}}} \right| = \left| \frac{\frac{N_f}{N_{\mathrm{MCS}}} - \frac{\widehat{N}_f}{N_{\mathrm{MCS}}}}{\frac{N_f}{N_{\mathrm{MCS}}}} \right| = \left| \frac{\widehat{N}_f}{N_f} - 1 \right| \tag{30}$$

where N_{MCS} is the sample size of MCS, N_f is the number of failure samples evaluated from the true performance function, and $\widehat{N}_f$ denotes the number of failure samples determined by the surrogate model (e.g. BSVR). In the random space Ω, let Ω_f denote the true failure region and Ω_s the safe region, whereas those predicted by the surrogate are represented as $\hat{\Omega}_f$ and $\hat{\Omega}_s$. Then, the failure sample size N_f in Eq. (30) can be calculated as:

$$N_f = \widehat{N}_f + \widehat{N}_{sf} - \widehat{N}_{fs} \tag{31}$$

where $\widehat{N}_{sf}$ is the number of MCS samples in Ω_f while falling into $\hat{\Omega}_s$ predicted by the surrogate model, and $\widehat{N}_{fs}$ is the number of MCS samples in Ω_s while falling into $\hat{\Omega}_f$ in the prediction. Since the established surrogate model itself is a Gaussian random process, thus the $\widehat{N}_{sf}$ and $\widehat{N}_{fs}$ being predicted also follow some probabilistic distribution. In this regard, a confidence interval can be assigned to the failure sample size N_f:

$$N_f \in \left[\widehat{N}_f - \widehat{N}_{fs}^u, \quad \widehat{N}_f + \widehat{N}_{sf}^u \right] \tag{32}$$

where $\widehat{N}_{fs}^u$ and $\widehat{N}_{sf}^u$ are the upper bounds of the confidence interval of $\widehat{N}_{fs}$ and $\widehat{N}_{sf}$. Accordingly, the maximum relative error of the failure probability estimation can be expressed as:

$$\epsilon_r \leq \max\left(\left| \frac{\widehat{N}_f}{\widehat{N}_f - \widehat{N}_{fs}^u} - 1 \right|, \left| \frac{\widehat{N}_f}{\widehat{N}_f + \widehat{N}_{sf}^u} - 1 \right| \right) = \hat{\epsilon}_{\max} \tag{33}$$

Assuming that the sample size in $\hat{\Omega}_f$ and $\hat{\Omega}_s$ are sufficiently large, $\widehat{N}_{fs}^u$ and $\widehat{N}_{sf}^u$ are respectively determined as the upper confidence interval of a Poisson distribution and a normal distribution in [74, 75]. However, this assumption may not be valid since the number of uncertain points decreases with the convergence of the learning process. Thus, an improved version of ESC using the bootstrap confidence estimation (BCE) has recently been developed in [76].

In the BCE-based ESC, only the samples with large probability of wrong sign prediction are considered instead of the whole population, in that the estimation error of failure probability is mainly contributed by these samples. Given a certain confidence interval, the highly uncertain samples near the LSS are defined as follows [76]:

$$\begin{aligned} \mathbf{X}_f &= \{ \boldsymbol{x} \mid \widehat{\mu}(\boldsymbol{x}) \leq 0; \widehat{\mu}(\boldsymbol{x}) + \alpha \widehat{\sigma}(\boldsymbol{x}) > 0 \} \\ \mathbf{X}_s &= \{ \boldsymbol{x} \mid \widehat{\mu}(\boldsymbol{x}) > 0; \widehat{\mu}(\boldsymbol{x}) - \alpha \widehat{\sigma}(\boldsymbol{x}) < 0 \} \end{aligned} \tag{34}$$

where $\mathbf{X}_f$ (with a sample size of n_f) represents the samples in $\hat{\Omega}_f$ while falling into $\hat{\Omega}_s$ with a certain confidence interval, and $\mathbf{X}_s$ (with a sample size of n_s) represents the samples in $\hat{\Omega}_s$ while falling into $\hat{\Omega}_f$ with a certain confidence interval. Considering the statistical property of the prediction model, each sample in $\mathbf{X}_f$ and $\mathbf{X}_s$ has a probability of wrong sign prediction, which is calculated as:

$$P_i^{\mathrm{wsp}} = \Phi\left(-\left|\frac{\hat{\mu}(\boldsymbol{x}_i)}{\hat{\sigma}(\boldsymbol{x}_i)}\right|\right), \boldsymbol{x}_i \in \hat{\Omega}_f \cup \hat{\Omega}_s \tag{35}$$

where P_i^{wsp} is the probability of wrong sign prediction at point $\boldsymbol{x}_i$. Hence, the upper bound values $\widehat{N}_{sf}^u$ and $\widehat{N}_{fs}^u$ can be calculated by means of bootstrap resampling method. Specifically, n_f samples are generated from $\mathbf{X}_f$ (correspondingly, n_s samples from $\mathbf{X}_s$) with replacement, after which the P_i^{wsp} for each sample can be calculated before computing their mean value $\bar{P}$. This process is repeated M times and the values of $\bar{P}$ are sorted in ascending order. Then, the confidence intervals of $\widehat{N}_{sf}$ and $\widehat{N}_{fs}$ can be expressed as:

$$CI_{\widehat{N}_{sf}} \in \left[n_f \bar{P}_{k_1}, n_f \bar{P}_{k_2}\right]_{\widehat{N}_{sf}}, CI_{\widehat{N}_{fs}} \in \left[n_s \bar{P}_{k_1}, n_s \bar{P}_{k_2}\right]_{\widehat{N}_{fs}} \tag{36}$$

where k_1 and k_2 are the rankings of the sorted values $\bar{P}$ corresponding to a confidence level α, that is,

$$k_1 = \left[M \times \frac{\alpha}{2}\right], k_2 = \left[M \times \left(1 - \frac{\alpha}{2}\right)\right] \tag{37}$$

where the repeated times is taken as $M = 1000$.

Therefore, with a predefined threshold ϵ_{tol} for the relative estimation error, the BCE-based ESC can be expressed as follows:

$$\epsilon_r \leq \max\left(\left|\frac{\widehat{N}_f}{\widehat{N}_f - \widehat{N}_{fs}^u} - 1\right|, \left|\frac{\widehat{N}_f}{\widehat{N}_f + \widehat{N}_{sf}^u} - 1\right|\right) = \hat{\epsilon}_{\max} \leq \epsilon_{tol} \tag{38}$$

where the upper bound values $\widehat{N}_{fs}^u$ and $\widehat{N}_{sf}^u$ can easily be retrieved from Eq. (36). It is referred to [74–76] and references therein for more information about the ESC and BCE-based ESC, both of which are originally developed for Kriging-based approaches. In this study, only the BCE-based ESC will be used to develop the hybrid convergence criterion and further adapt to the proposed ABSVR.

4. The proposed new learning function

In structural reliability analysis, the evaluation of failure probability is essentially a classification problem whose estimation error is mainly contributed by samples reside around the LSS, i.e. $\Omega_0 = \{\boldsymbol{x} \in \chi : G(\boldsymbol{x}) = 0\}$, especially in regions with high prediction variance $\hat{\sigma}(\boldsymbol{x})$ and large probability density $f_{\boldsymbol{X}}(\boldsymbol{x})$. Therefore, learning functions capable of identifying sample points with these desire properties are of critical importance to ensure the overall accuracy of the adaptive algorithm. In this regard, the learning process of an adaptive algorithm can be formulated as the following

optimization problem to search for the most informative samples:

$$\begin{aligned} &\text{find} && \boldsymbol{x}^* \\ &\max && \widehat{\sigma}(\boldsymbol{x})\rho(\boldsymbol{x})d_{\min}(\boldsymbol{x}) \\ &\text{s.t.} && \left|\widehat{\mu}(\boldsymbol{x})\right| = 0 \\ & && d_{\min}(\boldsymbol{x}) > d_t \end{aligned} \tag{39}$$

where $\widehat{\mu}$ and $\widehat{\sigma}$ are respectively the prediction mean and variance of the surrogate model, e.g. Eqs. (24-27) for the two BSVR models; $d_{\min}(\boldsymbol{x})$ is the minimum distance of point $\boldsymbol{x}$ to those in the current DoE, and d_t denotes the specified threshold distance; $\rho(\boldsymbol{x})$ represents the value of joint PDF $f_{\boldsymbol{X}}(\boldsymbol{x})$ evaluated at $\boldsymbol{x}$. According to the given information on distribution function, $\rho(\boldsymbol{x})$ can be calculated in different ways, that is,

$$\rho(\boldsymbol{x}) = \begin{cases} f_X(\boldsymbol{x}) & \text{with known joint PDF} \\ \prod_i^n f_i(x_i) & \text{with uncorrelated random variables} \\ c\left(F_1\left(x_1\right), F_2\left(x_2\right), \cdots, F_n\left(x_n\right)\right) \prod_i^n f_i(x_i) & \text{with correlated random variables} \end{cases} \tag{40}$$

where $f_i(\boldsymbol{x})$ and $F_1\left(x_1\right)$ are the marginal PDF and the corresponding cumulative distribution function (CDF) of x_i, with x_i being the ith element of random vector $\boldsymbol{x}$; and $c(\cdot)$ is the copula density function.

Specifically, the equality constraint $\left|\widehat{\mu}(\boldsymbol{x})\right| = 0$ in Eq. (39) ensures that the optimal solutions are points located on the LSS (at least very close to), whereas the inequality constraint $d_{\min}(\boldsymbol{x}) > d_t$ is solved to select samples with distances larger than a specified value from the existing ones in DoE. Therefore, solving the constrained optimization problem expressed in Eq. (39) can provide informative samples for model updating. This, however, would introduce additional optimization algorithm into the learning process and complicate the adaptive algorithm, hence making the approach less user-friendly. To bypass this limitation, a sampling-based learning function capable of selecting informative samples from the candidate sampling pool is proposed in this section. Following the idea of the penalty function method, the proposed learning function utilizes a simple yet effective way to guide the search toward critical points near the LSS with large probability density. Besides, a distance constraint term is introduced into the learning function to control the density of samples, thus avoids the clustering of samples in DoE. Moreover, the inclusion of prediction variance in the learning function enables the efficient exploration of the regions with large uncertainty. The formulation of the proposed learning function is elucidated in the following subsections.

4.1. Identification of samples near the LSS in critical regions

In order to select new sample point $\boldsymbol{x}_{\text{new}}$ on the LSS, a simple yet effective way is to transform the equality constraint $\left|\widehat{\mu}(\boldsymbol{x})\right| = 0$ into an approximate unconstrained optimization problem by introducing a penalty term to the function. One possible formulation is given as follows:

$$\boldsymbol{x}_{\text{new}} = \arg\min_{\boldsymbol{x}\in\boldsymbol{S}_C} \left\{ 1 + \vartheta \left(\frac{\left|\widehat{\mu}(\boldsymbol{x})\right|}{1 + \text{median}\left(\left|\widehat{\mu}(\boldsymbol{x})\right|\right)} \right)^{\tau} \right\} \tag{41}$$

where $\boldsymbol{S}_C$ is the candidate sampling pool generated by SRS; ϑ is a sufficiently large value that enables the penalty effect to work, which is taken as $\vartheta = 10^{12}$ in this study; τ denotes a positive scale factor ($\tau \geq 1$) to amplify the difference among the predicted values; the median $\left(\left|\widehat{\mu}(\boldsymbol{x})\right|\right)$ returns the median value of the absolute predictions at $\boldsymbol{S}_C$, which is introduced to reduce the magnitude effect to improve the flexibility of the algorithm. In this formula, the objective function tends to the minimum when $\left|\widehat{\mu}(\boldsymbol{x})\right| = 0$, i.e. for points located on the LSS, while becoming larger for points deviate further from the LSS. Therefore, the points in the vicinity of LSS can effectively be identified from the candidate samples $\boldsymbol{S}_C$.

To enable the selection of sample points in the critical regions, i.e. regions with relatively large prediction uncertainty and probability density, the objective function in Eq. (41) is reformulated by adding the effects of BSVR prediction variance $\widehat{\sigma}^2(\boldsymbol{x})$ and joint PDF $f_{\mathbf{X}}(\boldsymbol{x})$ into the formulation, that is,

$$\boldsymbol{x}_{\text{new}} = \arg\min_{\boldsymbol{x}\in\boldsymbol{S}_C} \left\{ \frac{1 + 10^{12}\left(\frac{\left|\widehat{\mu}(\boldsymbol{x})\right|}{1+\text{median}\left(\left|\widehat{\mu}(\boldsymbol{x})\right|\right)}\right)^{\tau}}{\left(1+\frac{\widehat{\sigma}(\boldsymbol{x})}{\sigma_{max}}\right)\cdot\left(1+\frac{\rho(\boldsymbol{x})}{\rho_{max}}\right)} \right\} \tag{42}$$

where $\sigma_{max} = max(\widehat{\sigma}(\boldsymbol{x}))$ is the maximum value of the standard deviation of BSVR model evaluated at $\boldsymbol{S}_C$; $\rho(\boldsymbol{x})$ is given in Eq. (40), and $\rho_{max} = max(\rho(\boldsymbol{x}))$. Learning through this function enables the identification of new sample points close to the LSS with large probability density and prediction variance, which is expected to greatly enhance the performance of BSVR-based reliability analysis.

4.2. A distance-based constraint

The learning process is highly likely to introduce points located too close to the existing ones in DoE when the learning function is formulated to focus only on points near the LSS in critical regions. These points contain little extra information for the refinement of the surrogate model, but can dramatically increase the computational burden. To address this issue, the distance constraint in Eq. (39) is further integrated into the learning function developed in the previous subsection, i.e. Eq. (42), to avoid the clustering of sample points in DoE.

The Euclidean distance is employed here to measure the distance between two points. Given a point $\boldsymbol{x}_C^i$ in the candidate set $\boldsymbol{S}_C$ (with a sample size of N_C) and a point $\boldsymbol{x}_D^j$ in the DoE $\boldsymbol{S}_D$ (with a sample size of N_D), the minimum distance of each sample point in $\boldsymbol{S}_C$ to those in $\boldsymbol{S}_D$ is calculated as:

$$d_{\min}(\boldsymbol{x}_C^i) = \min\left\{ \sqrt{\left(\boldsymbol{x}_C^i - \boldsymbol{x}_D^j\right)^{\mathrm{T}}\left(\boldsymbol{x}_C^i - \boldsymbol{x}_D^j\right)} \right\}, i = 1,2,\cdots,N_C; j = 1,2,\cdots,N_D \tag{43}$$

with $\boldsymbol{d}_{\min} = \left\{ d_{\min}(\boldsymbol{x}_C^1), d_{\min}(\boldsymbol{x}_C^2), \ldots, d_{\min}(\boldsymbol{x}_C^{N_C}) \right\}$ denoting the vector of the minimum distances.

It is important to define a reasonable value for the threshold distance d_t, in that d_t serves as an indicator of how close the new sample point is allowed to those in DoE. In the present study, the maximum of the minimum distance

between sample points in the current DoE is applied to define the threshold distance d_t, which is given as:

$$d_t = \omega \max\left\{\min\left(\sqrt{\left(\boldsymbol{x}_i - \boldsymbol{x}_j\right)^{\mathrm{T}}\left(\boldsymbol{x}_i - \boldsymbol{x}_j\right)}\right)\right\}, i = 1, 2, \ldots, N_D; j = 1, 2, \ldots, i-1, i+1, \ldots, N_D \tag{44}$$

where ω is a scale factor generally takes the value in the range of $[0.1, 0.5]$.

With the threshold distance d_t and minimum distances $\boldsymbol{d}_{\min}$ defined, the original distance constraint in Eq. (39) is recasted in the following form to facilitate the sample-based learning process:

$$\arg\max_{\boldsymbol{x}\in\boldsymbol{S}_C}\left\{\frac{1 + d_{\min}(\boldsymbol{x}_C^i)}{1 + \exp\left(-\delta\left(\frac{\left(d_{\min}(\boldsymbol{x}_C^i) - d_t\right)}{d_t}\right)\right)}\right\}, i = 1, 2, \cdots, N_C \tag{45}$$

where δ is a positive integer that determines the penalty degree when the distance constraint is violated, and is taken as $\delta = 30$ in this paper. Specifically, this formula favors the points with large distance to those in DoE (i.e. $d_{\min}(\boldsymbol{x}_C^i) > d_t$), while penalizes those being close to the existing ones (i.e. $d_{\min}(\boldsymbol{x}_C^i) < d_t$). By doing so, the density of samples in DoE can effectively be controlled and accordingly, the clustering of samples is avoided.

4.3. The new learning function

Integrating the distance-based constraint in Eq. (45) into the learning function as expressed in Eq. (42), a new Sampling-based Learning Function (SLF) capable of identifying informative points that disperse as far as possible from the existing ones can be devised as:

$$\text{SLF}: \quad \boldsymbol{x}_{\text{new}} = \arg\min_{\boldsymbol{x}\in\boldsymbol{S}_C}\left\{\frac{1 + 10^{12}\left(\frac{\left|\widehat{\mu}(\boldsymbol{x})\right|}{1+\text{median}\left(\left|\widehat{\mu}(\boldsymbol{x})\right|\right)}\right)^{\tau}}{\left(1 + \frac{\widehat{\sigma}(\boldsymbol{x})}{\sigma_{max}}\right)\cdot\left(1 + \frac{\rho(\boldsymbol{x})}{\rho_{max}}\right)\cdot\left(\frac{1+d_{\min}(\boldsymbol{x}_C^i)}{1+\exp\left(-30\left(\frac{\left(d_{\min}(\boldsymbol{x}_C^i) - d_t\right)}{d_t}\right)\right)}\right)}\right\} \tag{46}$$

Unlike the well-known learning function U which cannot be used for points located exactly on the LSS, i.e. $\left|\widehat{\mu}(\boldsymbol{x})\right| = 0$, the proposed learning function SLF still works for this particular case. To further improve the convergence speed of the learning process, the Sobol sequences are generated as the candidate samples $\boldsymbol{S}_C$ given its uniformity and space-filling property. It is noted that other low-discrepancy sequences can also be used for the same purpose.

5. A hybrid stopping criterion

The use of BCE-based stopping criterion (BCE-based ESC) as described in § 3.2 can greatly enhance the computational efficiency with the upper bound of estimation error controlled at a specified level. However, there are cases that the accuracy of the failure probability estimation tends to stabilize before the BCE-based ESC is satisfied, which

implies that adding additional samples after this stage will not contribute much to the improvement of the surrogate model, but rather increase the computational burden of the algorithm. To alleviate the potentially high computational cost, a hybrid stopping criterion able to detect the stabilization stage of failure probability estimation during the learning process is developed in this section.

To effectively detect the stabilization stage of failure probability estimation, a feasible way is to define a criterion utilizing the reliability indices acquired in consecutive iterations. In this study, three consecutive estimations (when the iteration number $i \geq 5$) are employed for this purpose, that is:

$$\left|\frac{\widehat{\beta}_i - \widehat{\beta}_{i-1}}{\widehat{\beta}_{i-1}}\right| < \epsilon_{tol1}, \quad \left|\frac{\widehat{\beta}_{i-1} - \widehat{\beta}_{i-2}}{\widehat{\beta}_{i-2}}\right| < \epsilon_{tol1} \quad \text{and} \quad \left|\frac{\widehat{\beta}_{i-2} - \widehat{\beta}_{i-3}}{\widehat{\beta}_{i-3}}\right| < \epsilon_{tol1}, i \geq 5 \tag{47}$$

where $\widehat{\beta}_i$, $\widehat{\beta}_{i-1}$, $\widehat{\beta}_{i-2}$ and $\widehat{\beta}_{i-3}$ are the reliability indices (i.e. $\widehat{\beta} = -\Phi^{-1}\left(\widehat{P_f}\right)$, with $\Phi^{-1}(\cdot)$ denoting the inverse of standard normal CDF) estimated in the current, the $(i-1)$th, the $(i-2)$th and the $(i-3)$th iterations, respectively; and ϵ_{tol1} is the convergence threshold defined in the range of $[10^{-5}, 10^{-3}]$. However, directly applying Eq. (47) as a stopping criterion may lead to inaccurate failure probability estimation due to premature of the learning process. Therefore, the BCE-based stopping criterion is integrated with Eq. (47) to derive a new one:

$$\begin{cases} \left|\frac{\widehat{\beta}_i - \widehat{\beta}_{i-1}}{\widehat{\beta}_{i-1}}\right| < \epsilon_{tol1}, \quad \left|\frac{\widehat{\beta}_{i-1} - \widehat{\beta}_{i-2}}{\widehat{\beta}_{i-2}}\right| < \epsilon_{tol1} \quad \text{and} \quad \left|\frac{\widehat{\beta}_{i-2} - \widehat{\beta}_{i-3}}{\widehat{\beta}_{i-3}}\right| < \epsilon_{tol1}, i \geq 5 \\ \max\left(\left|\frac{\widehat{N}_f}{\widehat{N}_f - \widehat{N}^u_{fs}} - 1\right|, \left|\frac{\widehat{N}_f}{\widehat{N}_f + \widehat{N}^u_{sf}} - 1\right|\right) = \hat{\epsilon}_{\max} \leq \epsilon_{tol2} \end{cases} \tag{48}$$

where the predefined threshold $\epsilon_{tol2} \in [0.005, 0.1]$ can generally lead to a good trade-off between accuracy and efficiency.

Similarly, an additional stabilization detection term is added to the original BCE-based ESC (i.e. Eq. (38)), that is,

$$\begin{cases} \max\left(\left|\frac{\widehat{N}_f}{\widehat{N}_f - \widehat{N}^u_{fs}} - 1\right|, \left|\frac{\widehat{N}_f}{\widehat{N}_f + \widehat{N}^u_{sf}} - 1\right|\right) = \hat{\epsilon}_{\max} \leq \epsilon_{tol3} \\ \left|\frac{\widehat{\beta}_i - \widehat{\beta}_{i-1}}{\widehat{\beta}_{i-1}}\right| < \epsilon_{tol4}, i \geq 5 \end{cases} \tag{49}$$

where ϵ_{tol3} and ϵ_{tol4} are the given threshold values for the BCE-based ESC and the stabilization detection term, respectively. In this criterion, the BCE-based ESC will not be activated until the stability condition is fulfilled.

It is noteworthy that although Eq. (48) is similar to Eq. (49) in the form, they are defined for different purpose. Specifically, Eq. (48) is mainly defined to avoid unnecessary calls once the failure probability estimation is detected to have stabilized with a certain precision, whereas Eq. (49) is defined to control the estimation error and thus ensure the overall accuracy of the algorithm. To achieve this, the ϵ_{tol1} in Eq. (48) is set to a smaller value than the ϵ_{tol4} in Eq. (49), e.g. $\epsilon_{tol1} = 10^{-4}$ and $\epsilon_{tol4} = 10^{-3}$; while the BCE-based ESC threshold ϵ_{tol2} in Eq. (48) is set to a larger value than its counterpart defined in Eq. (49), e.g. $\epsilon_{tol2} = 0.1$ and $\epsilon_{tol3} = 0.01$.

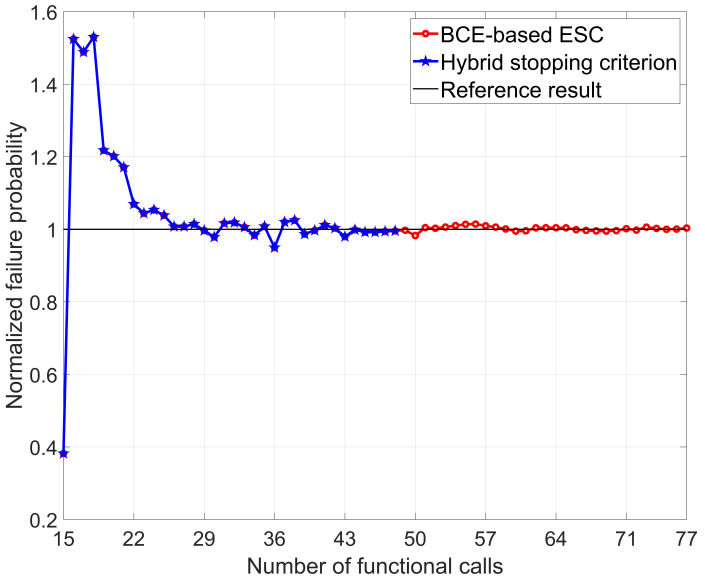

Figure 4: Convergence of the failure probability using different stopping criteria.

Therefore, the proposed hybrid stopping criterion consists of two separate criteria as expressed in Eq. (48) and Eq. (49), and the active learning process is terminated when any one of them is fulfilled. An example is shown in Fig. 4 to illustrate the potential gain of this hybrid stopping criterion as compared with the original BCE-based ESC. In this example, $\epsilon_{tol1} = \epsilon_{tol4} = 10^{-3}$, $\epsilon_{tol2} = 0.1$ and $\epsilon_{tol3} = 0.05$ for the hybrid criterion; $\epsilon_{tol} = 0.05$ for BCE-based ESC. It is seen that the failure probability has stabilized before the BCE-based ESC is fulfilled, and the proposed approach can detect this phenomenon and stop the algorithm with a reduced number of functional calls.

6. Implementation procedure of ABSVR

Combining the advanced schemes, the proposed learning function and the hybrid stopping criterion with the BSVR model, two Adaptive algorithms based on the BSVR (ABSVR) are proposed in this study, namely the one based on SLF (ABSVR1) and the one based on EISLF (ABSVR2). These two ABSVR methods start from a small initial DoE and iteratively refine the BSVR model by progressively enriching the DoE according to the proposed learning function. The learning process is repeated until the hybrid stopping criterion is met, then the failure probability can easily be estimated from the established BSVR model. Obviously, the only difference between ABSVR1 and ABSVR2 is the loss function used to construct the BSVR model. The flowchart of the ABSVR methods is depicted in Fig. 5 with 8 steps as summarized below:

- Step 1: Initialization of the algorithm. The parameters in ABSVR are initialized, including the sample size N_C in the candidate set $\boldsymbol{S}_C$, the sample size N_0 in the initial DoE, the coefficient α in the sampling region scheme (Eq. (29)) and the coefficient ω in the distance-based constraint (Eq. (44)), the positive scale factor τ in the learning function (Eq. (46)), and the convergence thresholds $\epsilon_{toli}, i = 1, 2, 3, 4$ in Eq. (48) and Eq. (49).

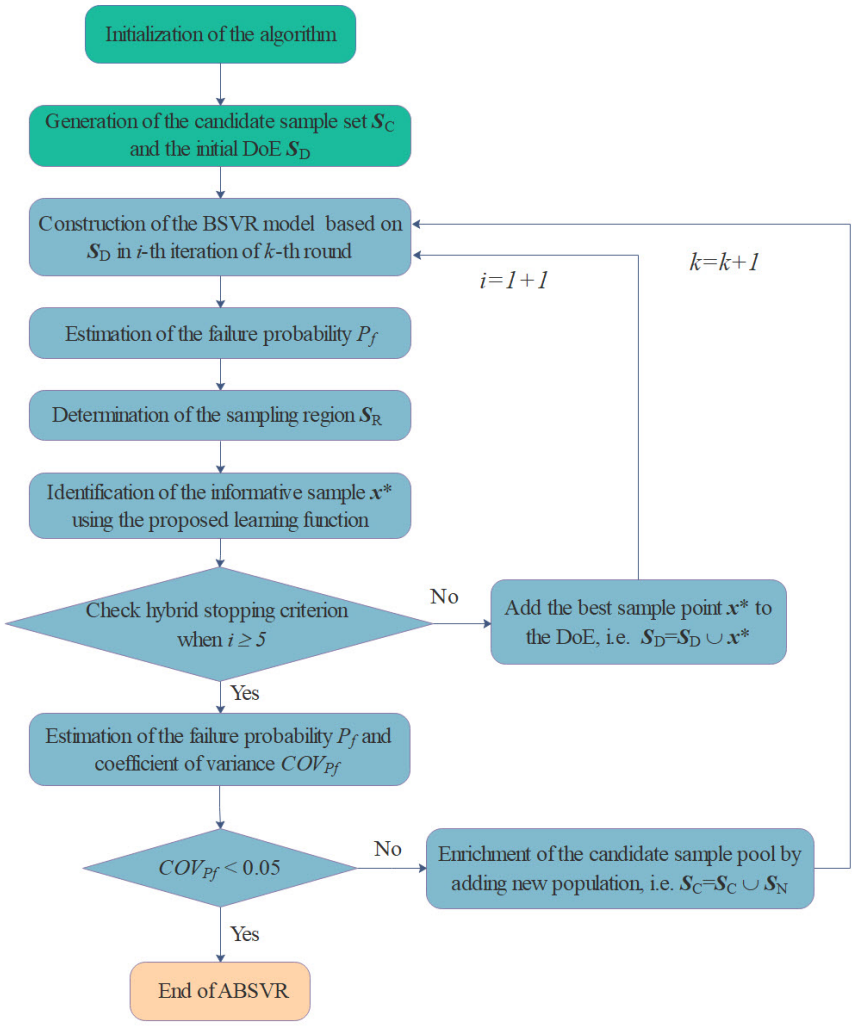

Figure 5: Flowchart of the ABSVR.

- Step 2: Generation of the candidate sample set $\boldsymbol{S}_C$ and initial DoE $\boldsymbol{S}_D$. To generate the Sobol sequence for $\boldsymbol{S}_C$, the UQLab [93] is employed in this study. Samples in the initial DoE are generated using Latin hypercube sampling (LHS) with a sample size of $N_0 = 15$.

- Step 3: Construction of the BSVR model. The generated DoE $\boldsymbol{S}_D$ is applied to build the BSVR model, based on which the prediction mean $\mu_{\hat{g}}(\boldsymbol{x})$ and variance $\sigma^2_{\hat{g}}(\boldsymbol{x})$ of the samples in $\boldsymbol{S}_C$ can be evaluated from Eq. (24) and Eq. (25) for ABSVR1, and from Eq. (26) and Eq. (27) for ABSVR2.

- Step 4: Generation of the reduced sample set $\boldsymbol{S}_R$ through the sampling region scheme expressed in Eq. (29). The failure probability is evaluated according to Eq. (3) with the true model being replaced by the BSVR model, and the points in $\boldsymbol{S}_R$ is obtained by filtering out the sample points with rather small probability density in $\boldsymbol{S}_C$.

- Step 5: Selection of informative samples to enrich the DoE. In each iteration, the sample point $\boldsymbol{x}^*$ in $\boldsymbol{S}_R$ that minimize the learning function Eq. (46) is selected as the optimal one, whose model response is evaluated by

calling the true performance function. Therefore, each time the DoE is enriched with the new sample point ($\boldsymbol{S}_D = \boldsymbol{S}_D \cup \boldsymbol{x}^*$) and $N_0 = N_0 + 1$. This learning process is repeated (i.e. iteration number $i = i + 1$) from Step 3 to Step 5 until one of the conditions in the hybrid stopping criterion is fulfilled.

- Step 6: Computation of the coefficient of variation. To ensure that the sample size in $\boldsymbol{S}_C$ is large enough to provide reliable failure probability estimation $\hat{P}_f$, the coefficient of variation below 5% is acceptable:

$$Cov = \sqrt{\frac{1 - \widehat{P}_f}{N_C \widehat{P}_f}} < 0.05 \tag{50}$$

- Step 7: Enrichment of the population in $\boldsymbol{S}_C$. If the condition in Eq. (50) is not met, $\boldsymbol{S}_C$ is enriched with new sample population $\boldsymbol{S}_N$, and the learning algorithm goes back to Step 3 and carries on until all the stopping criteria are fulfilled; otherwise, proceed to Step 8.

- Step 8: End of ABSVR. If the stopping condition expressed in Eq. (50) is met, the whole learning algorithm is terminated and the failure probability is evaluated on the final BSVR model.

7. Numerical examples

To illustrate the accuracy, efficiency and robustness of the proposed method, six numerical examples are tested in this section. The first example is a highly nonlinear problem. The second example considers a series system with three most probable points. The last four examples examine the applicability of ABSVRs to engineering structures, including a nonlinear oscillator, a roof truss, a suspension bridge and a cantilever tube. To show the robustness of the ABSVR, all results are obtained by averaging over 10 repeated runs of the algorithm, including the failure probability $\hat{P}_f$, the reliability index $\widehat{\beta}$, the total number of functional calls N_f and the relative error of failure probability $\epsilon_{\hat{P}_f}$. These results are compared with those of MCS and other existing methods whenever possible. In this paper, the relative error of failure probability $\epsilon_{\hat{P}_f}$ is calculated as:

$$\epsilon_{\hat{P}_f}(\%) = \frac{\left|\widehat{P}_f - \hat{P}_f^{MCS}\right|}{\hat{P}_f^{MCS}} \times 100\% \tag{51}$$

where $\hat{P}_f^{MCS}$ denotes the reference result provided by MCS, $\widehat{P}_f$ is the failure probability estimated from methods other than MCS, e.g. FORM, SORM and AK-MCS+U.

To make a trade-off between accuracy and efficiency of the algorithm, the application examples in this section are based on the settings illustrated in Table 1, if not specified otherwise.

Table 1
Parameter settings of ABSVR

Methods	$\hat{P}_f$
Initial sample size N_0	15
Coefficient α in SRS	0.1
Scale factor ω	0.3
Convergence threshold ϵ_{tol1}	1.0×10^{-4}
Convergence threshold ϵ_{tol2}	1.0×10^{-1}
Convergence threshold ϵ_{tol3}	1.2×10^{-2}
Convergence threshold ϵ_{tol4}	1.0×10^{-3}

7.1. Example 1: A highly nonlinear problem

This example considers a 2D high nonlinearity problem with a single failure region, which has been studied in [47, 52, 76]. The performance function of this problem is formulated as:

$$g(\boldsymbol{x}) = 1.2 - \frac{1}{20}\left(x_1^2 + 4\right)\left(x_2 - 1\right) + \sin\left(\frac{5}{2}x_1\right) \tag{52}$$

where x_1 and x_2 are two independent standard normal variables.

Following the procedures as described in § 6, the failure probability can easily be calculated by ABSVR1 and ABSVR2. However, it is noted that in the learning function Eq. (50) τ is a user-defined parameter, whose effect on the failure probability estimation should be investigated in order to determine a suitable value. In this regard, the boxplot of failure probabilities and corresponding functional calls are depicted in Fig. 6 and Fig. 7 for both ABSVR1 and ABSVR2, with τ taking different values, i.e. $\tau = 1$, $\tau = 2$,, $\tau = 4$, $\tau = 6$ and $\tau = 8$. It is observed from Fig. 6 that all results provided by ABSVR1 using different τ are in close agreement with the MCS result (red dotted line), and the maximum error is $\epsilon_{\hat{P}_f} = 0.7\%$ ($\tau = 1$). The largest variation of functional calls shows up when $\tau = 8$, whereas the highest efficiency is achieved when $\tau = 4$. Similar conclusions can be drawn for ABSVR2, as shown in Fig. 7. Therefore, the scale factor τ has certain effects on the performance of ABSVRs, while $\tau = 4$ can generally reach a good trade-off between accuracy and efficiency. For the sake of brevity, only the results of ABSVR1 and ABSVR2 with $\tau = 4$ will be employed to show the performance of ABSVR for structural reliability analysis.

The results of these two ABSVRs are compared with those provided by MCS, FORM, SORM, AK-MCS+U\AK-MCS+EFF [48], REIF\REIF2 [52] and AK-SDMCS [69], as summarized in Table 2. The reference result of this example is obtained by means of MCS with 1×10^6 samples, i.e. $\widehat{P}_f = 4.71 \times 10^{-3}$ with a coefficient of variation $\delta_{P_f} = 1.45\%$, which is directly taken from [52]. It is seen from Table 2 that FORM is unable to deliver accurate failure probability prediction for this case, in that the nonlinear failure features cannot be captured by the first-order Talyor expansion, hence leading to an estimation error $\epsilon_{\hat{P}_f} > 100\%$. Although the accuracy of FORM can significantly be improved by SORM, the relative error is still unacceptably high, i.e. 22.06%, let alone more functional calls are required. On the contrary, all the investigated adaptive algorithms, including the Kriging-based approaches and the proposed BSVR-based ones, are capable of providing accurate failure probability prediction with high efficiency, i.e.

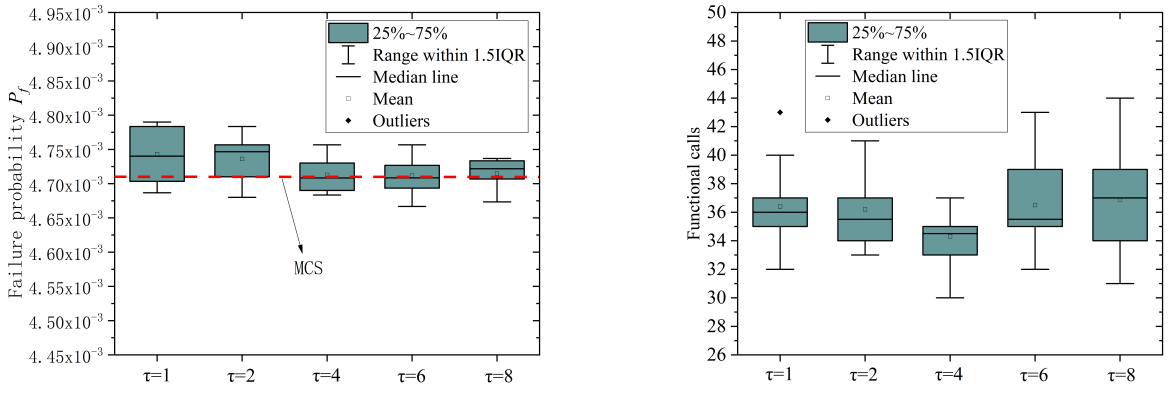

(a) (b)

Figure 6: Boxplot of the results for ABSVR1 using different values of τ: (a) The failure probability estimation; (b) The functional calls. (For interpretation of the references to color in this figure, please refer to the web version of this article.)

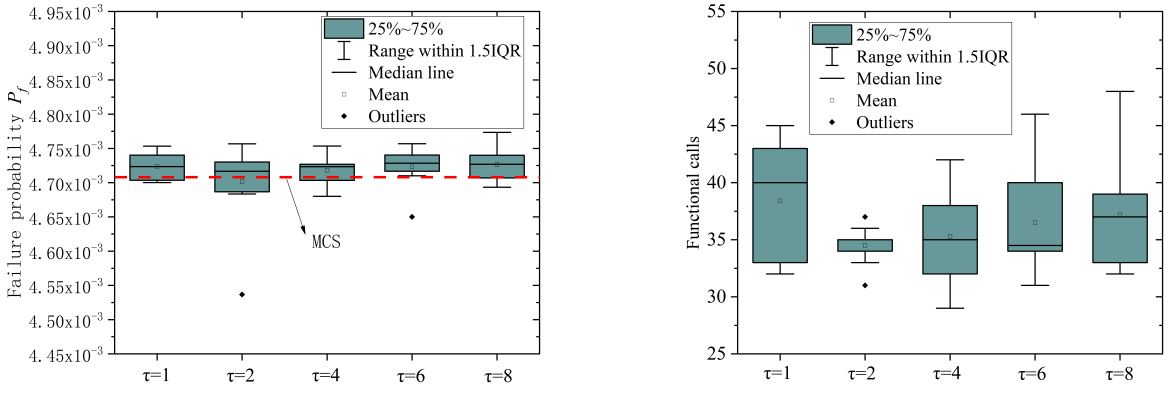

(a) (b)

Figure 7: Boxplot of the results for ABSVR2 using different values of τ: (a) The failure probability estimation; (b) The functional calls. (For interpretation of the references to color in this figure, please refer to the web version of this article.)

the relative error $\epsilon_{\hat{P}_f}$ is less than 1% with no more than 50 functional calls. Among these adaptive algorithms, the two proposed ABSVRs and the REIF2 exhibit better performance both in terms of accuracy and efficiency, indicating the effectiveness of ABSVRs for a problem with high nonlinearity.

To further illustrate the superior performance of ABSVRs, the converged BSVR models and the convergence history of failure probability corresponding to a single run of ABSVR1 and ABSVR2 are plotted in Fig. 8 and Fig. 9, respectively. It is observed from Fig. 8a and Fig. 9a that all the newly selected sample points (blue triangles with sequence number) are located in the vicinity of LSS and spread uniformly without clustering, resulting in an excellent match of the established BSVR models with the true one in critical regions. Accordingly, fast convergence of the failure

Table 2
Results of reliability analysis for Example 1 using different methods

Methods	$\hat{P}_f$	$\hat{\beta}$	N_f	$\epsilon_{\hat{P}_f}(\%)$
MCS	4.710×10^{-3}	2.5964	1×10^{6}	–
FORM	2.563×10^{-2}	1.9492	779	>100
SORM	3.671×10^{-3}	2.6809	791	22.06
REIF	4.720×10^{-3}	2.5957	42.3	0.23
REIF2	4.710×10^{-3}	2.5964	35.6	0.03
AK-MCS+U	4.689×10^{-3}	2.5980	49.4	0.45
AK-MCS+EFF	4.742×10^{-3}	2.5941	49.8	0.67
AK-SDMCS	4.667×10^{-3}	2.5997	41.3	0.92
ABSVR1	4.713×10^{-3}	2.5966	34.3	0.06
ABSVR2	4.718×10^{-3}	2.5954	35.3	0.17

Note: Here, $\tau = 4$ for both ABSVR1 and ABSVR2; the results of REIF and REIF2 are directly taken from [52]; the results of FORM and SORM are calculated by means of UQLab [94].

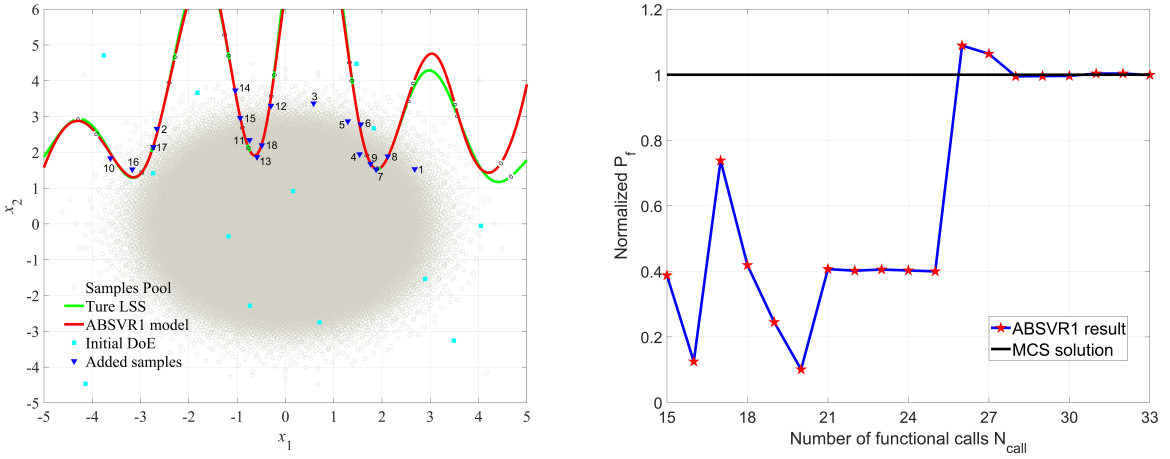

(a) (b)

Figure 8: Results from a single run of ABSVR1: (a) The converged BSVR model; (b) The convergence history of failure probability. (For interpretation of the references to color in this figure, please refer to the web version of this article.)

probability estimation is observed after fluctuating significantly in the first 13 iterations, as shown in Fig. 8b and Fig. 9b. These results demonstrate the effectiveness of the proposed learning function (i.e. SLF) for identifying informative samples. Moreover, it is noteworthy that the LSS being poorly approximated at locations with low probability densities does not necessarily result in a poor estimation of the failure probability, in that the regions with extremely weak probability densities have little contribution to the prediction result.

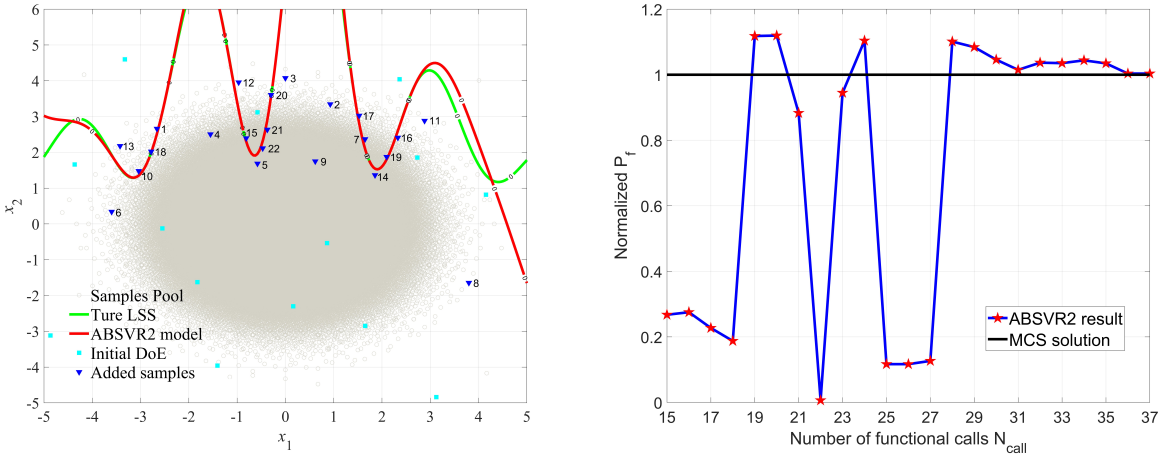

(a) (b)

Figure 9: Results from a single run of ABSVR2: (a) The converged BSVR model; (b) The convergence history of failure probability. (For interpretation of the references to color in this figure, please refer to the web version of this article.)

7.2. Example 2: A series system with four branches

The second example is a series system with four branches, whose performance function is given as follows [48, 76]:

$$g(\boldsymbol{x}) = \min \begin{Bmatrix} 3 + 0.1\left(x_1 - x_2\right)^2 - \frac{x_1+x_2}{\sqrt{2}} \\ 3 + 0.1\left(x_1 - x_2\right)^2 + \frac{x_1+x_2}{\sqrt{2}} \\ \left(x_1 - x_2\right) + \frac{7}{\sqrt{2}} \\ \left(x_2 - x_1\right) + \frac{7}{\sqrt{2}} \end{Bmatrix} \tag{53}$$

where x_1 and x_2 are two standard normal random variables. The failure probability of this series system are calculated by the proposed ABSVRs with $\tau = 4$ and compared with various other methods, among which the MCS (with a sample size of 1×10^7) reported in [76] is used as the reference result, i.e. $\hat{P}_f = 2.221 \times 10^{-3}$ with a coefficient of variation smaller than $\delta_{P_f} = 1\%$. The results of AK-MCS+U and AK-MCS+EFF [48], Neural Network-based Importance Sampling (NNIS) [95], Neural Network-based Directional Simulation (NNDS) [95], Active Deep Neural Network method (ADNN) [46] and ESC+RLCB [76] from the corresponding references are also listed for comparison purpose, as shown in Table 3.

One can see from Table 3 that the results calculated from traditional one-shot sampling schemes, namely the NNIS and the NNDS exhibit large estimation errors, i.e. respectively with a relative error of 30.57% and 54.98%, even at the expense of larger computational effort. In contrast to these non-adaptive algorithms, the estimation carried out by adaptive algorithms can generally achieve a good trade-off between accuracy and efficiency. Specifically, the proposed ABSVR1 and ABSVR2 provide comparable results (slightly better) on failure probability using much fewer model evaluations as compared with AK-MCS+U and AK-MCS+EFF, and reach higher precision than ADNN with less

Table 3
Results of reliability analysis for Example 2 using different methods

Methods	$\hat{P}_f$	$\hat{\beta}$	N_f	$\epsilon_{\hat{P}_f}(\%)$
MCS	2.221×10^{-3}	2.845	1×10^7	–
AK-MCS+U	2.233×10^{-3}	2.843	96	0.54
AK-MCS+EFF	2.232×10^{-3}	2.843	101	0.50
NNIS	2.900×10^{-3}	2.760	125	30.57
NNDS	1.000×10^{-3}	3.050	67	54.98
ADNN	2.192×10^{-3}	2.849	70	1.31
ESC+RLCB	2.265×10^{-3}	2.839	43.8	1.98
ABSVR1	2.218×10^{-3}	2.845	47.3	0.13
ABSVR2	2.224×10^{-3}	2.844	43.9	0.13

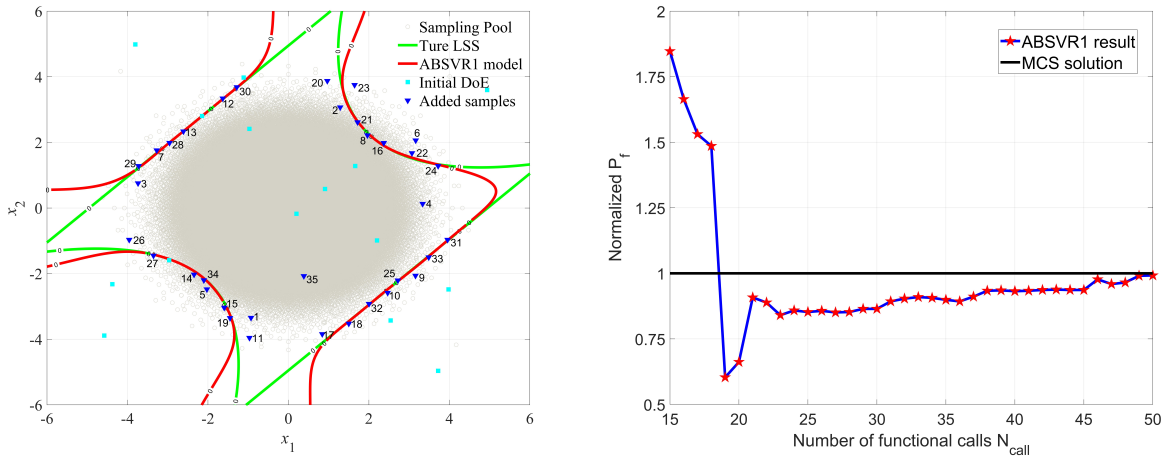

(a) (b)

Figure 10: Results from a single run of ABSVR1: (a) The converged BSVR model; (b) The convergence history of failure probability. (For interpretation of the references to color in this figure, please refer to the web version of this article.)

functional calls.

The converged BSVR models and the convergence history of failure probability corresponding to a single run of ABSVR1 and ABSVR2 are depicted in Fig. 10 and Fig. 11, respectively. As can be seen from Fig. 10a and Fig. 11a that the initial sampling points (cyan square points) in DoE are spread over the random space, whereas the newly enriched points (blue triangles with sequence number) are uniformly distributed along the LSS in the regions of interest. This implies that the proposed SLF is capable of guiding the search toward a converged BSVR model that perfectly matches with the true one in the critical regions, leading to the fast convergence of both ABSVR1 and ABSVR2 for failure probability estimation, as shown in Fig. 10b and Fig. 11b. Similar to Example 1, the poor fitting property of BSVR model in regions with rather low probability density (i.e. the four corners) will not mitigate the prediction accuracy since their contribution to failure probability is negligible.

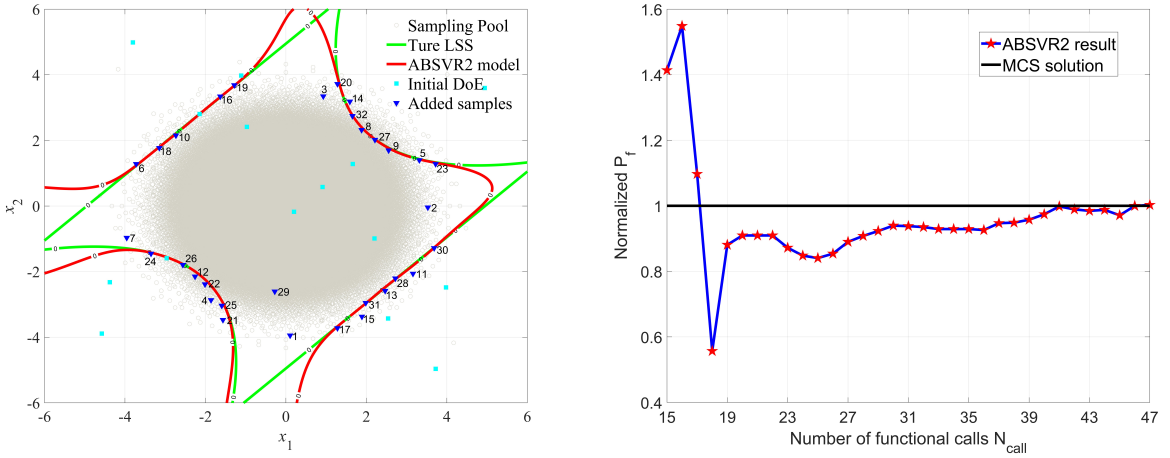

(a) (b)

Figure 11: Results from a single run of ABSVR2: (a) The converged BSVR model; (b) The convergence history of failure probability. (For interpretation of the references to color in this figure, please refer to the web version of this article.)

Table 4
Statistical information of the random variables

Random variable	Distribution	Mean	Standard deviation
m	Normal	1	0.05
c_1	Normal	1	0.1
c_2	Normal	0.1	0.01
r	Normal	0.5	0.05
F_1	Normal	1	0.2
t_1	Normal	1	0.2

7.3. Example 3: Dynamic response of a nonlinear oscillator

This example considers a nonlinear oscillator subjected to a rectangular load pulse, as shown in Fig 6. It is an undamped single degree of freedom system, which has been investigated in numerous studies [37, 48, 58, 68, 73]. The performance function of this nonlinear system is expressed as:

$$g\left(c_1, c_2, m, r, t_1, F_1\right) = 3r - \left|\frac{2F_1}{m\omega_0^2}\sin\left(\frac{\omega_0 t_1}{2}\right)\right| \tag{54}$$

where $\omega_0 = \sqrt{\left(c_1 + c_2\right)/m}$, and the distribution parameters of these random variables are listed in Table 4.

The reference result of this example is calculated from MCS with a sample size of 1×10^7 and the corresponding failure probability is 2.859×10^{-2}. The results calculated from FORM and SORM, and those by adaptive Kriging approaches, namely the AK-MCS\AK-MCSi\AK-MSS [65], and the AK-SS\AWL-MCS [58] directly taken from the corresponding references are also used for comparison purpose, as summarized in Table 5 along with the results provided by the proposed ABSVRs with $\tau = 4$.

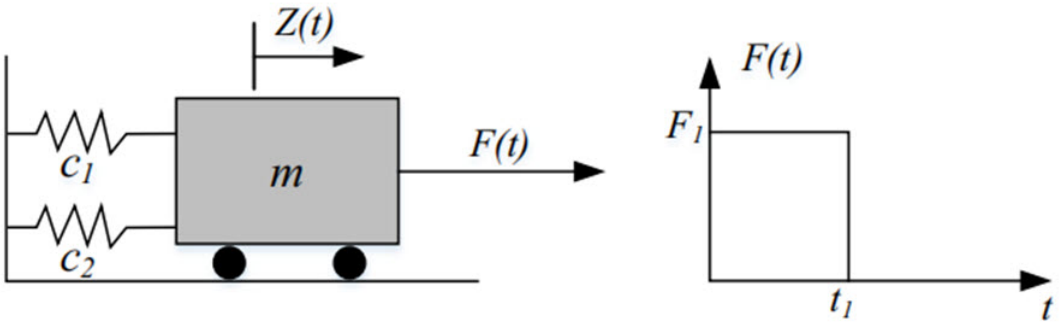

Figure 12: Nonlinear oscillator subjected to a rectangular load pulse.

Table 5
Results of reliability analysis for Example 3 using different methods

Methods	$\hat{P}_f$	$\hat{\beta}$	N_f	$\epsilon_{\hat{P}_f}(\%)$
MCS	2.859×10^{-2}	1.902	1×10^7	–
FORM	3.108×10^{-2}	1.865	48	8.71
SORM	2.900×10^{-2}	1.896	128	1.43
AK-MCS	2.852×10^{-2}	1.903	530	0.24
AK-SS	2.833×10^{-2}	1.906	410	0.91
AK-MCSi	2.830×10^{-2}	1.906	85	1.01
AK-MSS	2.870×10^{-2}	1.900	86	0.38
AWL-MCS	2.826×10^{-2}	1.907	65	1.15
ABSVR1	2.855×10^{-2}	1.903	46.8	0.15
ABSVR2	2.871×10^{-2}	1.900	45.4	0.41

Note: The results of FORM and SORM are calculated by means of UQLab [94]; the results of AK-MCS, AK-MCSi and AK-MSS are directly taken from [65]; those of AK-SS and AWL-MCS are taken from [58] .

One can see from Table 5 that the failure probability estimated by FORM exhibits the largest error (i.e. $\epsilon_{\hat{P}_f} = 8.71\%$) among the investigated methods, albeit its high efficiency for this particular case. The accuracy of FORM can be improved by SORM, but at the expense of substantially higher computational effort than FORM, i.e. the total number of functional calls N_f increased from 48 to 128. Although AK-MCS and AK-SS both exhibit high precision, i.e. respectively with a relative error $\epsilon_{\hat{P}_f} = 0.24\%$ and $\epsilon_{\hat{P}_f} = 0.91\%$, the required number of functional calls is prohibitively high compared with other adaptive algorithms. On the contrary, the other three adaptive Kriging-based approaches, namely the AK-MCSi, the AK-MSS and the AWL-MCS are capable of providing a balanced performance for this case. Remarkably, the proposed ABSVR1 and ABSVR2 show excellent performance both in terms of accuracy and efficiency, i.e. with a relative error less than 0.5% using less than 50 functional calls, indicating the capability of ABSVRs to reach a balanced performance for structural reliability analysis of this dynamic system. The convergence history of failure probability by three independent runs of ABSVRs are depicted in Fig. 13, where the estimation results are seen to have quickly converged to the reference solution for both ABSVR1 and ABSVR2 after fluctuated significantly in the first 12 iterations.

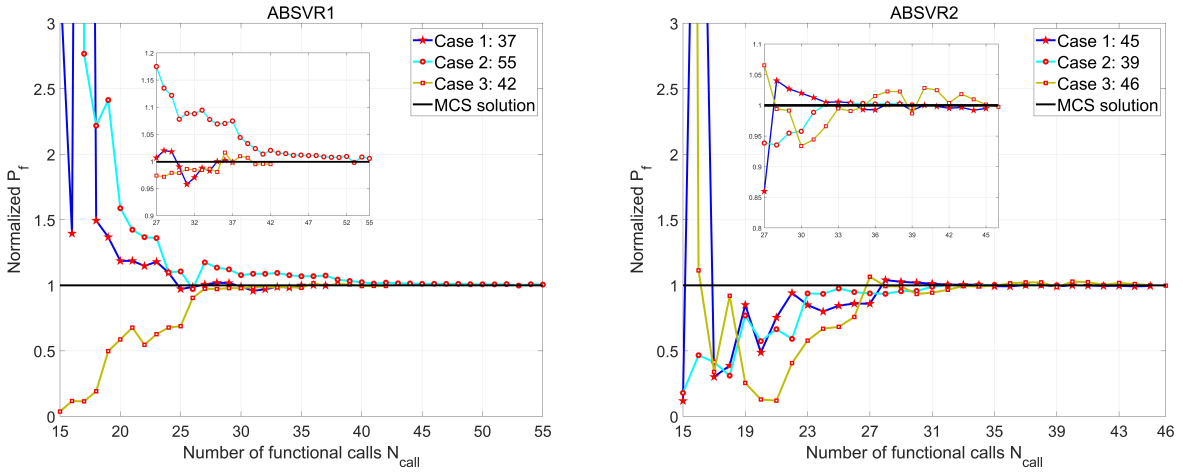

(a) (b)

Figure 13: The convergence history of failure probability: (a) Prediction by ABSVR1; (b) Prediction by ABSVR2. (For interpretation of the references to color in this figure, please refer to the web version of this article.)

7.4. Example 4: A suspension bridge under vessel-bridge collision

To test the applicability of the ABSVRs in bridge engineering, a suspension bridge under vessel-bridge collision is considered in this example, which is adapted from [96, 97]. The general view of this bridge is shown in Fig. 14, where the span arrangement is 154m + 452m + 154m with a navigation width of 211.52m. According to the finite element analysis conducted in [96], the failure model of the bridge south pier is induced by the violation of ultimate lateral resistance. Thus, the performance function corresponds to this failure model can be expressed in terms of the ultimate lateral resistance of the pier and vessel impact force as follows:

$$g(V_T, V_{\min}, \Omega, \Theta, D_{WT}) = -0.19\Omega\Theta - 0.61\Omega - 5.01\Theta + 31.76 - 0.122V\sqrt{D_{WT}} \tag{55}$$

where V_T and $V_{\min}$ respectively denote typical impact velocity and minimum design impact velocity; Ω is the water level; Θ represent the impact angle; D_{WT} is the deadweight tonnage of the vessel; and V is the design impact velocity which can be calculated as follows:

$$V = \begin{cases} V_T & x_0 \leqslant 52.875 \\ \frac{x_L V_T - x_c V_{\min} - x_0(V_T - V_{\min})}{x_L - x_c} & 52.875 \leqslant x_0 \leqslant 513 \\ V_{\min} & x_0 > 513 \end{cases} \tag{56}$$

where x_0 is the distance from the face of pier to the centerline of channel and $x_0 = 173.12$m is defined in this study. The statistical information of these random variables are listed in Table 6.

The results of failure probability estimation using various methods are summarized in Table 7, where the reference result is averaged over 10 independent runs of MCS with 1×10^6 sample points, and the results of FORM, SORM, IS, SS and AK-MCS are calculated using UQLab [94] by default settings. One can see from Table 7 that the precision of

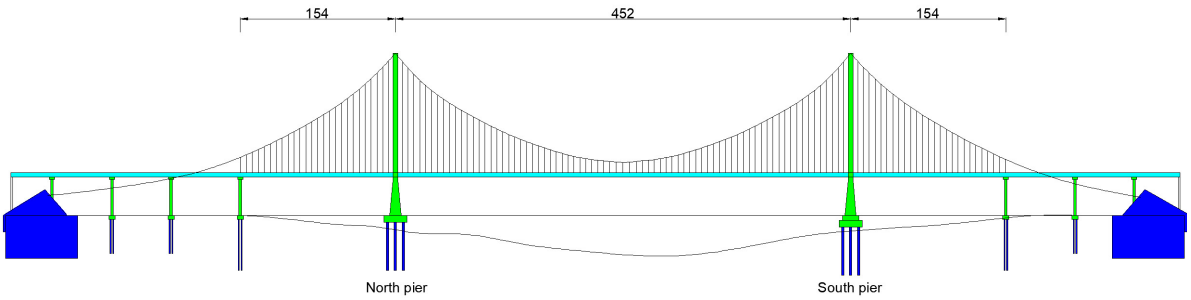

Figure 14: General view of the suspension bridge (adapted from [96, 97]).

Table 6
Statistical information of the random variables

Random variable	Distribution	Mean	Standard deviation
V_T(m/s)	Normal	3	0.6
$V_{\min}$(m/s)	Normal	1	0.2
Θ(°)	Gumbel	10	4
Ω(m)	Normal	1.32	0.264
D_{WT}(t)	Lognormal	3067	1962.88

Table 7
Results of reliability analysis for Example 4 using different methods

Methods	$\hat{P}_f$	$\hat{\beta}$	N_f	$\epsilon_{\hat{P}_f}(\%)$
MCS	2.192×10^{-2}	2.016	1×10^{6}	–
FORM	2.299×10^{-2}	1.996	42	4.88
SORM	2.208×10^{-2}	2.013	99	0.73
IS	2.310×10^{-2}	1.994	1042	5.38
SS	2.130×10^{-2}	2.028	1900	2.83
AK-MCS	2.203×10^{-2}	2.014	170	0.50
ABSVR1	2.174×10^{-2}	2.019	36.8	0.81
ABSVR2	2.231×10^{-2}	2.008	74.8	1.79

FORM is relatively low, albeit its high efficiency for this case. SORM can greatly improve the accuracy of FORM, yet at the expense of more functional calls. Although the advanced simulation methods such as IS and SS generally show good performance for structural reliability analysis, their accuracy and efficiency are poor for this particular case. Among the adaptive algorithms, the AK-MCS achieves the highest precision, i.e. $\epsilon_{\hat{P}_f} = 0.5\%$, but requires more computational effort than the proposed ABSVRs. On the contrary, both of the ABSVR1 and ABSVR2 can achieve a balanced performance, with the ABSVR1 exhibits the best trade-off between accuracy and efficiency. The convergence history of failure probability by three independent runs of ABSVRs are depicted in Fig. 15, where the estimation result of ABSVR1 is seen to have quickly converged to the reference solution after fluctuated significantly in the first 8 iterations. However, the convergence speed of ABSVR2 is much lower than that of ABSVR2 for this case,

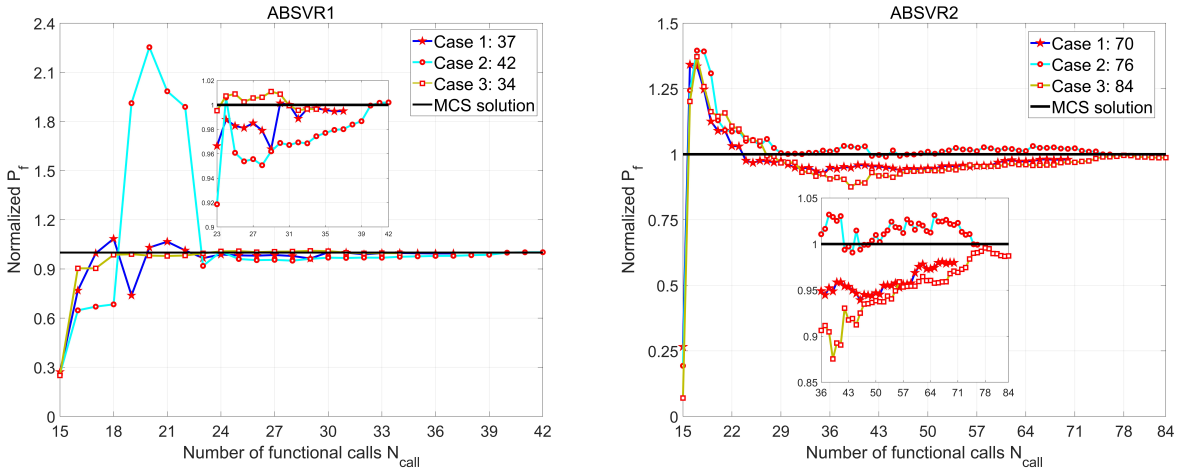

(a) (b)

Figure 15: The convergence history of failure probability: (a) Prediction by ABSVR1; (b) Prediction by ABSVR2. (For interpretation of the references to color in this figure, please refer to the web version of this article.)

i.e. the stabilized stage is observed after 50 iterations. Nevertheless, the ABSVR2 is still more efficient than SORM and AK-MCS to reach comparable accuracy.

7.5. Example 5: A roof truss structure

A roof truss structure as shown in Fig. 16 is investigated in this example. The bottom chords and tension bars of the roof truss are made of steel, while the material of the top chords and the compression bars is reel-reinforced concrete. The structure is subjected to a uniformly distributed load q, which is transformed into the concentrated force $P = ql/4$ applied on the nodes of the truss. The performance function of this truss structure corresponding to the vertical displacement of node C is defined as [58, 76, 98]:

$$g = v_t - \frac{ql^2}{2}\left(\frac{3.81}{A_c E_c} + \frac{1.13}{A_s E_s}\right) \tag{57}$$

where the threshold value v_t is taken as $v_t = 0.03$m; l is the length of the truss; A_c and A_s are the cross-sectional areas of the steel-reinforced concrete and the steel bars; E_c and E_s are the corresponding Young's modulus of the steel-reinforced concrete and the steel bars. The statistical information of these random variables are listed in Table 8.

For this example, the reference result is taken from [98], where the MCS with 1×10^6 sample points is employed to obtain the failure probability, i.e. $\hat{P}_f = 2.017 \times 10^{-3}$ with a coefficient of variation $\delta_{P_f} = 2.22\%$. The results obtained from the proposed ABSVRs with $\tau = 4$ are compared with those obtained by SORM, IS, AK-MCS+U, AK-MCS+EFF, and the failure-pursuing sampling (FPS)-based approaches (including FPS+U, FPS+EFF and FPS+RD) [98], which are all summarized in Table 9.

As can be seen from Table 9, the accuracy of IS is poor compared with other investigated methods, even at the expense of a larger number of functional calls. The accuracy of SORM is higher than IS with a reduced number of functional calls, yet the overall performance of the adaptive algorithms is still better than that of SORM. Among

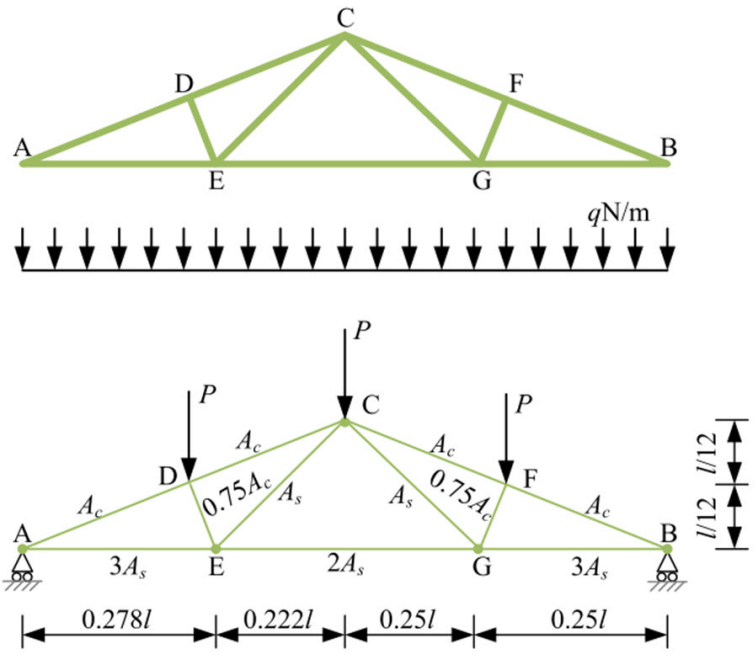

Figure 16: The schematic diagram of the roof truss (after [98]).

Table 8
Statistical information of the random variables

Random variable	Distribution	Parameter 1	Parameter 2
q(N/m)	Weibull	20000	500
l(m)	Lognormal	12.5	0.125
$A_s(m^2)$	Lognormal	9.82×10^{-4}	6×10^{-5}
$A_c(m^2)$	Lognormal	0.04	0.0035
E_s(Pa)	Lognormal	1×10^{11}	1×10^{9}
E_c(Pa)	Lognormal	2×10^{10}	1×10^{9}

Note: For Weibull distribution, parameters 1 and 2 are the scale and shape parameters, respectively, while they represent the mean and standard deviation for lognormal distribution.

the Kriging-based approaches, the performance of methods using learning function U (AK-MCS+U and FPS+U) is slightly worse than their counterparts using other learning functions (AK-MCS+EFF, FPS+EFF and FPS+RD), with the FPS+RD exhibits the best performance both in terms of accuracy and efficiency. Interestingly, the proposed ABSVR1 and ABSVR2 achieves the same level of accuracy as other adaptive Kriging methods with the least number of functional calls, indicating the improved performance of the proposed ABSVRs. The convergence history of failure probability by three independent runs of ABSVRs are depicted in Fig. 17, where the estimation results are seen to have quickly converged to the reference solution for both ABSVR1 and ABSVR2 after fluctuated significantly in the first 20 iterations.

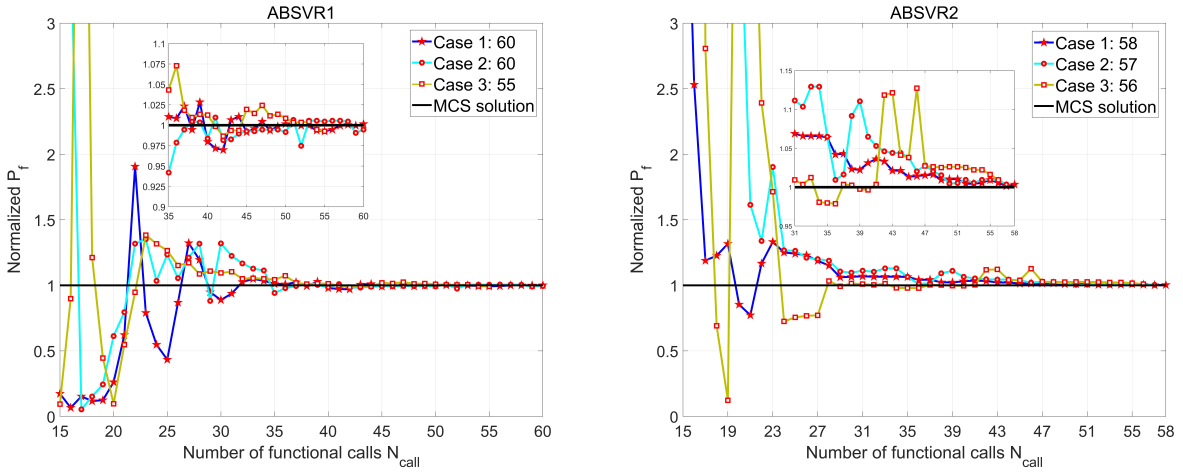

(a) (b)

Figure 17: The convergence history of failure probability: (a) Prediction by ABSVR1; (b) Prediction by ABSVR2. (For interpretation of the references to color in this figure, please refer to the web version of this article.)

Table 9
Results of reliability analysis for Example 5 using different methods

Methods	$\hat{P}_f$	$\hat{\beta}$	N_f	$\epsilon_{\hat{P}_f}(\%)$
MCS	2.017×10^{-3}	2.875	1×10^6	–
SORM	1.998×10^{-3}	2.878	198	0.94
IS	2.081×10^{-3}	2.866	1118	3.17
AK-MCS+U	2.007×10^{-3}	2.877	104.1	0.50
AK-MCS+EFF	2.018×10^{-3}	2.875	63.1	0.05
FPS+U	2.031×10^{-3}	2.873	80.25	0.69
FPS+EFF	2.019×10^{-3}	2.875	76.3	0.10
FPS+RD	2.018×10^{-3}	2.875	66.1	0.05
ABSVR1	2.027×10^{-3}	2.874	53.3	0.49
ABSVR2	2.022×10^{-3}	2.875	58.4	0.25

Note: The results of SORM and IS are calculated by UQLab [94]; the results of AK-MCS+U, AK-MCS+EFF and FPS-based methods are directly taken from [98].

7.6. Example 6: A cantilever tube

The last example considers a cantilever tube as shown in Fig. 18. This tube is subjected to three external forces F_1, F_2, P and one torsion T, and will fail when the yield strength σ is smaller than the maximum stress $\sigma_{\max}$. Thus, the performance function can be expressed as [73, 75, 99]:

$$g(\boldsymbol{x}) = \sigma - \sigma_{\max} \tag{58}$$

where $\sigma_{\max}$ is the maximum von Mises stress of the tube and is calculated as:

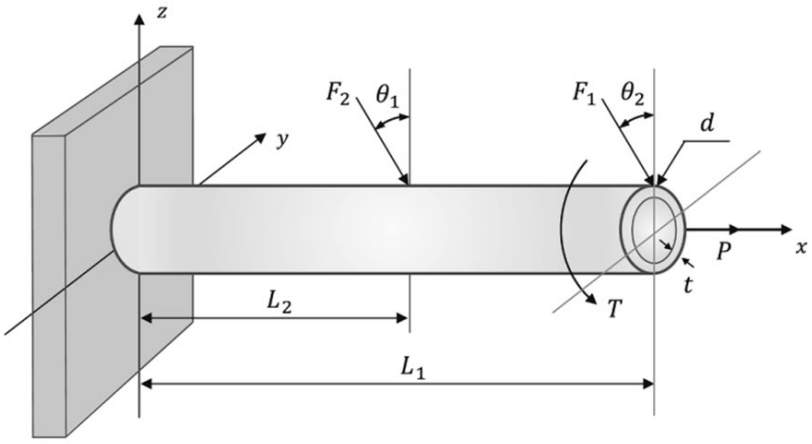

Figure 18: A cantilever tube (after [73]).

Table 10
Statistical information of the random variables

Random variable	Distribution	Parameter 1	Parameter 2
q(N/m)	Weibull	20000	500
l(m)	Lognormal	12.5	0.125
$A_s(m^2)$	Lognormal	9.82×10^{-4}	6×10^{-5}
$A_c(m^2)$	Lognormal	0.04	0.0035
E_s(Pa)	Lognormal	1×10^{11}	1×10^{9}
E_c(Pa)	Lognormal	2×10^{10}	1×10^{9}

Note: For Weibull distribution, parameters 1 and 2 are the scale and shape parameters, respectively, while they represent the mean and standard deviation for lognormal distribution.

$$\sigma_{\max} = \sqrt{\sigma_x^2 + 3\tau_{zx}^2} \tag{59}$$

where σ_x and τ_{zx} represent the normal stress and torsional stress on the top of surface of the tube at the origin, which are respectively given as:

$$\sigma_x = \frac{P + F_1 \sin\theta_1 + F_2 \sin\theta_2}{A} + \frac{Md}{2I} \tag{60}$$

$$\tau_{zx} = \frac{Td}{2J} \tag{61}$$

where A is the cross-sectional area, M denotes the bending moment and I represents the moment of inertia. These parameters can be calculated as:

$$M = F_1 L_1 \cos\theta_1 + F_2 L_2 \cos\theta_2 \tag{62}$$

Table 11
Results of reliability analysis for Example 6 using different methods

Methods	$\hat{P}_f$	$\widehat{\beta}$	N_f	$\epsilon_{\hat{P}_f}(\%)$
MCS*	6.850×10^{-3}	2.465	6×10^{4}	–
AK-MCS+EFF	6.850×10^{-3}	2.465	84	0
REAK	6.817×10^{-3}	2.467	59	0.49
ISKRA	6.850×10^{-3}	2.846	71	0
MCS	7.093×10^{-3}	2.453	1×10^{6}	–
ABSVR1	7.109×10^{-3}	2.452	37.7	0.22
ABSVR2	7.088×10^{-3}	2.453	37.1	0.08

Note: The reference result MCS* in [75] is obtained by MCS with a population size of 6×10^{4}, based on which the relative error of AK-MCS+EFF, REAK and ISKRA are calculated.

$$A = \frac{\pi}{4}\left[d^2 - (d-2t)^2\right] \tag{63}$$

$$I = \frac{\pi}{64}\left[d^4 - (d-2t)^4\right] \tag{64}$$

$$J = 2I \tag{65}$$

A total of 9 random variables are involved in this example and their statistical information is listed in Table 8. The results of failure probability estimation using the proposed ABSVR1 and ABSVR2 along with other methods are summarized in Table 11, in which the results of AK-MCS+EFF, REAK and ISKRA (and their estimation errors) are directly taken from [75]. The reference result of this example is averaged over 10 independent runs of MCS with 1×10^{6} sample points, giving the estimation of $\widehat{P}_f = 7.093\times10^{-3}$ with a coefficient of variation $\delta_{P_f} = 1.45\%$. To reduce the variation of failure probability estimation among different algorithm runs, the ABSVRs are obtained by setting the convergence threshold $\epsilon_{tol3} = 0.008$, with other parameters remain the same as listed in Table 1.

As can be seen from Table 11 that all the results provided by these investigated methods are in good agreement with their corresponding reference ones. It is noteworthy that due to different number of samples used in [75] and the present study, the reference results are a bit different, i.e. the coefficient of variation δ_{P_f} for MCS* with 6×10^{4} samples is $\delta_{P_f} = 4.92\%$ and the one for MCS with 1×10^{6} samples is $\delta_{P_f} = 1.18\%$. Nevertheless, both the proposed ABSVRs and the REAK show a good trade-off between accuracy and efficiency for this case, i.e. reach a relative error within 0.5% using less than 50 functional calls. The convergence history of failure probability by three independent runs of ABSVRs are depicted in Fig. 19, where the estimation results are seen to have quickly converged to the reference solution for both ABSVR1 and ABSVR2 after fluctuated significantly in the first 9 iterations.

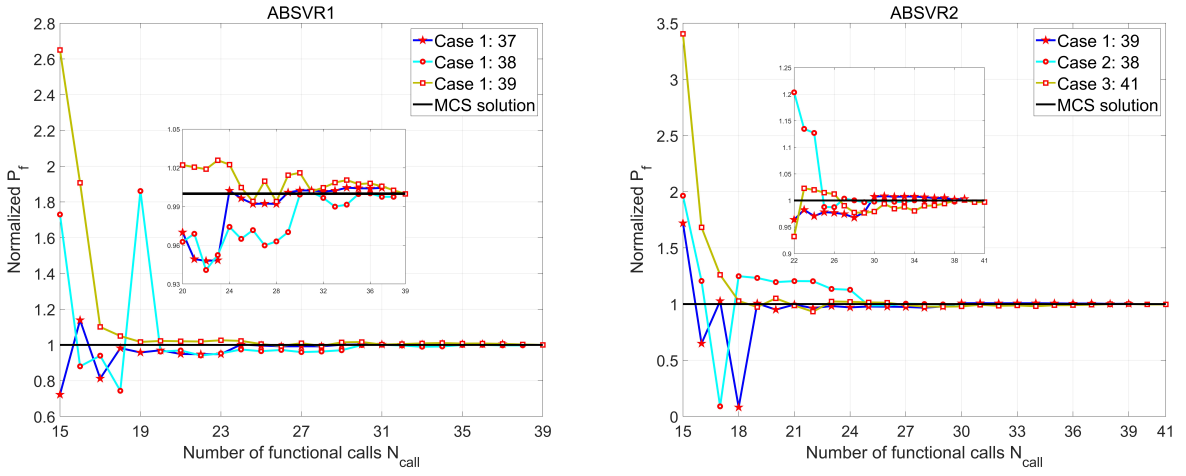

(a) (b)

Figure 19: The convergence history of failure probability: (a) Prediction by ABSVR1; (b) Prediction by ABSVR2. (For interpretation of the references to color in this figure, please refer to the web version of this article.)

8. Conclusions

In this paper, an adaptive algorithm based on Bayesian SVR (ABSVR) is proposed for efficient reliability analysis with high accuracy. According to the loss function employed to establish the BSVR model, two versions of ABSVR are proposed, namely the ABSVR1 based on square loss function and the ABSVR2 based on ε-insensitive square loss function. Following the idea of the penalty function method in optimization, a new learning function known as SLF is devised for effective selection of important sample points, e.g. points close to the LSS in critical regions with sufficient large probability density. To avoid the clustering of new enriched samples with the existing ones, a distance constraint term is added to the learning function to control the density of samples in DoE. Besides, the adaptive sampling region scheme originally developed for Kriging-based approach is adapted here to further enhance the computational efficiency by filtering out sample points with weak probability density, in that these samples have little contribution to the failure probability evaluation. Moreover, a hybrid stopping criterion based on error-based stopping criterion using the bootstrap confidence estimation is developed to terminate the active learning process, ensuring that the learning algorithm stops at an appropriate stage.

To illustrate the performance of the proposed ABSVRs for structural reliability analysis, six numerical examples including one system reliability problem and four engineering cases are investigated, the results of which are compared with those from other state-of-the-art reliability methods. The results have shown that both the proposed ABSVR1 and ABSVR2 are well-suited for structural reliability analysis, and capable of delivering failure probability estimation with better performance than other investigated methods, both in terms of accuracy and efficiency. Besides, the proposed learning function exhibit excellent performance for guiding the search toward informative samples close to the LSS and thus, contributing to the fast convergence of the failure probability evaluated from the BSVR model.

Overall, the proposed ABSVR is easy to implement since no embedded optimization algorithm nor iso-probabilistic transformation is required, and its applicability and effectiveness for structural reliability analysis have been validated

through numerical examples featuring different complexity. However, this work is still an early step towards applying Bayesian SVR for reliability analysis of complex engineering structures, the integration of ABSVR with more advanced simulation methods and dimension reduction techniques is worth exploring to deal with high-dimensional problems or rare failure events.

Acknowledgements

The financial support from the National Natural Science Foundation of China (No. 52078425), the National Science Fund for Distinguished Young Scholars (No. 51525804) and the NSF grant CMMI-1562244 are highly appreciated.

References

[1] Achintya Haldar and Sankaran Mahadevan. *Probability, reliability, and statistical methods in engineering design*. J. Wiley & Sons, Incorporated, 2000.

[2] Jie Li and Jianbing Chen. *Stochastic dynamics of structures*. John Wiley & Sons, 2009.

[3] Ikjin Lee, Yoojeong Noh, and David Yoo. A novel second-order reliability method (sorm) using noncentral or generalized chi-squared distributions. *Journal of Mechanical Design*, 134(10):100912, 2012.

[4] RH Lopez, AJ Torii, LFF Miguel, and JE Souza Cursi. Overcoming the drawbacks of the form using a full characterization method. *Structural Safety*, 54:57–63, 2015.

[5] Iason Papaioannou, Costas Papadimitriou, and Daniel Straub. Sequential importance sampling for structural reliability analysis. *Structural safety*, 62:66–75, 2016.

[6] Diego A Alvarez, Felipe Uribe, and Jorge E Hurtado. Estimation of the lower and upper bounds on the probability of failure using subset simulation and random set theory. *Mechanical Systems and Signal Processing*, 100:782–801, 2018.

[7] Yan-Gang Zhao and Tetsuro Ono. Moment methods for structural reliability. *Structural safety*, 23(1):47–75, 2001.

[8] Yan Shi, Zhenzhou Lu, Siyu Chen, and Liyang Xu. A reliability analysis method based on analytical expressions of the first four moments of the surrogate model of the performance function. *Mechanical Systems and Signal Processing*, 111:47–67, 2018.

[9] Jun Xu and Chao Dang. A novel fractional moments-based maximum entropy method for high-dimensional reliability analysis. *Applied Mathematical Modelling*, 75:749–768, 2019.

[10] Huiquan Miao, Wei Liu, and Jie Li. Seismic reliability analysis of water distribution networks on the basis of the probability density evolution method. *Structural Safety*, 86:101960, 2020.

[11] AA Chojaczyk, AP Teixeira, Luís C Neves, JB Cardoso, and C Guedes Soares. Review and application of artificial neural networks models in reliability analysis of steel structures. *Structural Safety*, 52:78–89, 2015.

[12] Tong Zhou, Yongbo Peng, and Jie Li. An efficient reliability method combining adaptive global metamodel and probability density evolution method. *Mechanical Systems and Signal Processing*, 131:592–616, 2019.

[13] Atin Roy, Ramkrishna Manna, and Subrata Chakraborty. Support vector regression based metamodeling for structural reliability analysis. *Probabilistic Engineering Mechanics*, 55:78–89, 2019.

[14] Frank Grooteman. An adaptive directional importance sampling method for structural reliability. *Probabilistic Engineering Mechanics*, 26(2):134–141, 2011.

[15] Vincent Dubourg, Bruno Sudret, and Franois Deheeger. Metamodel-based importance sampling for structural reliability analysis. *Probabilistic Engineering Mechanics*, 33:47–57, 2013.

[16] Jinsuo Nie and Bruce R Ellingwood. Directional methods for structural reliability analysis. *Structural Safety*, 22(3):233–249, 2000.

[17] Mohsen Ali Shayanfar, Mohammad Ali Barkhordari, Moien Barkhori, and Mohammad Barkhori. An adaptive directional importance sampling method for structural reliability analysis. *Structural Safety*, 70:14–20, 2018.

[18] HJ Pradlwarter, GI Schueller, Phaedon-Stelios Koutsourelakis, and Dimos C Charmpis. Application of line sampling simulation method to reliability benchmark problems. *Structural Safety*, 29(3):208–221, 2007.

[19] Chao Yin and Ahsan Kareem. Computation of failure probability via hierarchical clustering. *Structural Safety*, 61:67–77, 2016.

[20] Siu-Kui Au and James L Beck. Estimation of small failure probabilities in high dimensions by subset simulation. *Probabilistic engineering mechanics*, 16(4):263–277, 2001.

[21] Ziqi Wang, Marco Broccardo, and Junho Song. Hamiltonian monte carlo methods for subset simulation in reliability analysis. *Structural Safety*, 76:51–67, 2019.

[22] Abraham M Hasofer and Niels C Lind. Exact and invariant second-moment code format. *Journal of the Engineering Mechanics division*, 100(1):111–121, 1974.

[23] Xianzhen Huang, Yuxiong Li, Yimin Zhang, and Xufang Zhang. A new direct second-order reliability analysis method. *Applied Mathematical Modelling*, 55:68–80, 2018.

[24] Karl Breitung. Asymptotic approximations for multinormal integrals. *Journal of Engineering Mechanics*, 110(3):357–366, 1984.

[25] Armen Der Kiureghian, Hong-Zong Lin, and Shyh-Jiann Hwang. Second-order reliability approximations. *Journal of Engineering mechanics*, 113(8):1208–1225, 1987.

[26] Régis Lebrun and Anne Dutfoy. Do rosenblatt and nataf isoprobabilistic transformations really differ? *Probabilistic Engineering Mechanics*, 24(4):577–584, 2009.

[27] Jinsheng Wang, Muhannad Aldosary, Song Cen, and Chenfeng Li. Hermite polynomial normal transformation for structural reliability analysis. *Engineering Computations*, 2020.

[28] Chao Hu, Byeng D Youn, Pingfeng Wang, et al. *Engineering Design Under Uncertainty and Health Prognostics*. Springer, 2019.

[29] Muhannad Aldosary, Jinsheng Wang, and Chenfeng Li. Structural reliability and stochastic finite element methods: State-of-the-art review and evidence-based comparison. *Engineering Computations*, 35(6):2165–2214, 2018.

[30] U. Bucher, C.G.and Bourgund. A fast and efficient response surface approach for structural reliability problems. *Structural and Multidisciplinary Optimization*, 7(1):57–66, 1990.

[31] Somdatta Goswami, Shyamal Ghosh, and Subrata Chakraborty. Reliability analysis of structures by iterative improved response surface method. *Structural Safety*, 60:56–66, 2016.

[32] Géraud Blatman and Bruno Sudret. Adaptive sparse polynomial chaos expansion based on least angle regression. *Journal of Computational Physics*, 230(6):2345–2367, 2011.

[33] Emiliano Torre, Stefano Marelli, Paul Embrechts, and Bruno Sudret. Data-driven polynomial chaos expansion for machine learning regression. *Journal of Computational Physics*, 388:601–623, 2019.

[34] Irfan Kaymaz. Application of kriging method to structural reliability problems. *Structural Safety*, 27(2):133–151, 2005.

[35] Maliki Moustapha, Jean-Marc Bourinet, Benoît Guillaume, and Bruno Sudret. Comparative study of kriging and support vector regression for structural engineering applications. *ASCE-ASME Journal of Risk and Uncertainty in Engineering Systems, Part A: Civil Engineering*, 4(2):04018005, 2018.

[36] Jian Deng. Structural reliability analysis for implicit performance function using radial basis function network. *International journal of solids and structures*, 43(11-12):3255–3291, 2006.

[37] Jing Zhao, Chen Jianqiao, and Li Xu. Rbf-ga: An adaptive radial basis function metamodeling with genetic algorithm for structural reliability analysis. *Reliability Engineering and System Safety*, 189:42–57, 2019.

[38] Hyeongjin Song, Kyung K Choi, Ikjin Lee, Liang Zhao, and David Lamb. Adaptive virtual support vector machine for reliability analysis of high-dimensional problems. *Structural and Multidisciplinary Optimization*, 47(4):479–491, 2013.

[39] J.M. Bourinet. Rare-event probability estimation with adaptive support vector regression surrogates. *Reliability Engineering and System Safety*, 150:210–221, 2016.

[40] Atin Roy and Subrata Chakraborty. Support vector regression based metamodel by sequential adaptive sampling for reliability analysis of structures. *Reliability Engineering & System Safety*, page 106948, 2020.

[41] Jorge E.Hurtado and Diego A.Alvarez. Neural-network-based reliability analysis: a comparative study. *Computer Methods in Applied Me-*

chanics and Engineering, 191:113–132, 2001.

[42] A.M. Gomes, H.M.and Awruch. Comparison of response surface and neural network with other methods for structural reliability analysis. *Structural Safety*, 26(1):49–67, 2004.

[43] Giovanis D. G. Lagaros N.D.and Papadrakakis M. Papadopoulos, V. Accelerated subset simulation with neural networks for reliability analysis. *Computer Methods in Applied Mechanics and Engineering*, 223-224:70–80, 2012.

[44] Kai Cheng and Zhenzhou Lu. Structural reliability analysis based on ensemble learning of surrogate models. *Structural Safety*, 83:101905, 2020.

[45] Xu Li, Chunlin Gong, Liangxian Gu, Wenkun Gao, Zhao Jing, and Hua Su. A sequential surrogate method for reliability analysis based on radial basis function. *Structural Safety*, 73:42–53, 2018.

[46] Zhengliang Xiang, Jiahui Chen, Yuequan Bao, and Hui Li. An active learning method combining deep neural network and weighted sampling for structural reliability analysis. *Mechanical Systems and Signal Processing*, 140:106684, 2020.

[47] B. J. Bichon, M. S. Eldred, L. P. Swiler, S. Mahadevan, and J. M. Mcfarland. Efficient global reliability analysis for nonlinear implicit performance functions. *Aiaa Journal*, 46(10):2459–2468, 2008.

[48] B. Echard, N. Gayton, and M. Lemaire. Ak-mcs: An active learning reliability method combining kriging and monte carlo simulation. *Structural Safety*, 33(2):p.145–154, 2011.

[49] Benjamin Richard, Christian Cremona, and Lucas Adelaide. A response surface method based on support vector machines trained with an adaptive experimental design. *Structural safety*, 39:14–21, 2012.

[50] Hongzhe Dai, Hao Zhang, Wei Wang, and Guofeng Xue. Structural reliability assessment by local approximation of limit state functions using adaptive markov chain simulation and support vector regression. *Computer-Aided Civil and Infrastructure Engineering*, 27(9):676–686, 2012.

[51] Zhaoyan Lv, Zhenzhou Lu, and Pan Wang. A new learning function for kriging and its applications to solve reliability problems in engineering. *Computers and Mathematics with Applications*, 70(5):1182–1197, 2015.

[52] Xufang Zhang, Lei Wang, and John Dalsgaard Sorensen. Reif: A novel active-learning function toward adaptive kriging surrogate models for structural reliability analysis. *Reliability Engineering and System Safety*, 185(may):440–454, 2019.

[53] Yan Shi, Zhenzhou Lu, Ruyang He, Yicheng Zhou, and Siyu Chen. A novel learning function based on kriging for reliability analysis. *Reliability Engineering and System Safety*, 198:106857, 2020.

[54] Zhifu Zhu and Xiaoping Du. Reliability analysis with monte carlo simulation and dependent kriging predictions. *Journal of Mechanical Design*, 138(12), 2016.

[55] Abdul-Kader El Haj and Abdul-Hamid Soubra. Improved active learning probabilistic approach for the computation of failure probability. *Structural Safety*, 88:102011.

[56] Qiujing Pan and Daniel Dias. An efficient reliability method combining adaptive support vector machine and monte carlo simulation. *Structural Safety*, 67:85–95, 2017.

[57] Zhili Sun, Jian Wang, Rui Li, and Cao Tong. Lif: A new kriging based learning function and its application to structural reliability analysis. *Reliability Engineering and System Safety*, 157(Complete):152–165, 2017.

[58] Zeng Meng, Zhuohui Zhang, Gang Li, and Dequan Zhang. An active weight learning method for efficient reliability assessment with small failure probability. *Structural and Multidisciplinary Optimization*, 61(3):1157–1170, 2020.

[59] Gayton-N. Lemaire M. Echard, B. and N. Relun. A combined importance sampling and kriging reliability method for small failure probabilities with time-demanding numerical models. *Reliability Engineering and System Safety*, 111:232–240, 2013.

[60] Morio-J. Balesdent, M. and J. Marzat. Kriging-based adaptive importance sampling algorithms for rare event estimation. *Structural Safety*, 44:1–10, 2013.

[61] Weidong Chen, Chunlong Xu, Yaqin Shi, Jingxin Ma, and Shengzhuo Lu. A hybrid kriging-based reliability method for small failure probabilities. *Reliability Engineering and System Safety*, 189:31–41, 2019.

[62] Liu-Y. Chen B. Guo, Q. and Y. Zhao. An active learning kriging model combined with directional importance sampling method for efficient reliability analysis. *Probabilistic Engineering Mechanics*, 60:103054, 2020.

[63] Jingwen Song, Pengfei Wei, Marcos Valdebenito, and Michael Beer. Adaptive reliability analysis for rare events evaluation with global

imprecise line sampling. *Computer Methods in Applied Mechanics and Engineering*, 372:113344, 2020.

[64] Xiaoxu Huang, Jianqiao Chen, and Hongping Zhu. Assessing small failure probabilities by ak-ss: An active learning method combining kriging and subset simulation. *Structural Safety*, 59:86–95, 2016.

[65] Chunlong Xu, Weidong Chen, Jingxin Ma, Yaqin Shi, and Shengzhuo Lu. Ak-mss: An adaptation of the ak-mcs method for small failure probabilities. *Structural Safety*, 86:101971, 2020.

[66] J-M Bourinet, François Deheeger, and Maurice Lemaire. Assessing small failure probabilities by combined subset simulation and support vector machines. *Structural Safety*, 33(6):343–353, 2011.

[67] J-M Bourinet. Rare-event probability estimation with adaptive support vector regression surrogates. *Reliability Engineering & System Safety*, 150:210–221, 2016.

[68] Jian Wang, Zhili Sun, Runan Cao, and Yutao Yan. An efficient and robust adaptive kriging for structural reliability analysis. *Structural and Multidisciplinary Optimization*, pages 1–16, 2020.

[69] Maijia Su, Guofeng Xue, Dayang Wang, Yongshan Zhang, and Yong Zhu. A novel active learning reliability method combining adaptive kriging and spherical decomposition-mcs (ak-sdmcs) for small failure probabilities. *Structural and Multidisciplinary Optimization*, pages 1–23, 2020.

[70] Teixeira-A.P. Gaspar, B. and C.G. Soares. Adaptive surrogate model with active refinement combining kriging and a trust region method. *Reliability Engineering and System Safety*, 165:277–291, 2017.

[71] Pei-H. Liu H. Wen, Z. and Z. Yue. A sequential kriging reliability analysis method with characteristics of adaptive sampling regions and parallelizability. *Reliability Engineering and System Safety*, 153:170–179, 2016.

[72] Xufang Zhang, Lei Wang, and John Dalsgaard Sørensen. Akois: an adaptive kriging oriented importance sampling method for structural system reliability analysis. *Structural Safety*, 82:101876, 2020.

[73] Jungho Kim and Junho Song. Probability-adaptive kriging in n-ball (pak-bn) for reliability analysis. *Structural Safety*, 85:101924, 2020.

[74] Z. Wang and A. Shafieezadeh. Esc: an efficient error-based stopping criterion for kriging-based reliability analysis methods. *Structural and Multidisciplinary Optimization*, 59(5):1621–1637, 2019.

[75] Zeyu Wang and Abdollah Shafieezadeh. Reak: Reliability analysis through error rate-based adaptive kriging. *Reliability Engineering & System Safety*, 182:33–45, 2019.

[76] Jiaxiang Yi, Qi Zhou, Yuansheng Cheng, and Jun Liu. Efficient adaptive kriging-based reliability analysis combining new learning function and error-based stopping criterion. *Structural and Multidisciplinary Optimization*, pages 1–20, 2020.

[77] Barron J Bichon, John M McFarland, and Sankaran Mahadevan. Efficient surrogate models for reliability analysis of systems with multiple failure modes. *Reliability Engineering & System Safety*, 96(10):1386–1395, 2011.

[78] William Fauriat and Nicolas Gayton. Ak-sys: an adaptation of the ak-mcs method for system reliability. *Reliability Engineering & System Safety*, 123:137–144, 2014.

[79] Kai Yuan, Ning-Cong Xiao, Zhonglai Wang, and Kun Shang. System reliability analysis by combining structure function and active learning kriging model. *Reliability Engineering & System Safety*, 195:106734, 2020.

[80] Chen Jiang, Haobo Qiu, Liang Gao, Dapeng Wang, Zan Yang, and Liming Chen. Eek-sys: System reliability analysis through estimation error-guided adaptive kriging approximation of multiple limit state surfaces. *Reliability Engineering & System Safety*, page 106906, 2020.

[81] Ning-Cong Xiao, Hongyou Zhan, and Kai Yuan. A new reliability method for small failure probability problems by combining the adaptive importance sampling and surrogate models. *Computer Methods in Applied Mechanics and Engineering*, 372:113336, 2020.

[82] Tayyab Zafar, Yanwei Zhang, and Zhonglai Wang. An efficient kriging based method for time-dependent reliability based robust design optimization via evolutionary algorithm. *Computer Methods in Applied Mechanics and Engineering*, 372:113386, 2020.

[83] Zeng Meng, Zhuohui Zhang, Dequan Zhang, and Dixiong Yang. An active learning method combining kriging and accelerated chaotic single loop approach (ak-acsla) for reliability-based design optimization. *Computer Methods in Applied Mechanics and Engineering*, 357:112570, 2019.

[84] Roland Schöbi and Bruno Sudret. Structural reliability analysis for p-boxes using multi-level meta-models. *Probabilistic Engineering Mechanics*, 48:27–38, 2017.

[85] Ning-Cong Xiao, Kai Yuan, and Chengning Zhou. Adaptive kriging-based efficient reliability method for structural systems with multiple failure modes and mixed variables. *Computer Methods in Applied Mechanics and Engineering*, 359:112649, 2020.

[86] Stefano Marelli and Bruno Sudret. An active-learning algorithm that combines sparse polynomial chaos expansions and bootstrap for structural reliability analysis. *Structural Safety*, 75:67–74, 2018.

[87] Linxiong Hong, Huacong Li, and Kai Peng. A combined radial basis function and adaptive sequential sampling method for structural reliability analysis. *Applied Mathematical Modelling*, 90:375–393.

[88] Yicheng Zhou and Zhenzhou Lu. Active polynomial chaos expansion for reliability-based design optimization. *AIAA Journal*, 57(12):5431–5446, 2019.

[89] Kai Cheng and Zhenzhou Lu. Active learning bayesian support vector regression model for global approximation. *Information Sciences*, 544:549–563.

[90] Wei Chu, S Sathiya Keerthi, and Chong Jin Ong. Bayesian support vector regression using a unified loss function. *IEEE transactions on neural networks*, 15(1):29–44, 2004.

[91] Yicheng Zhou, Zhenzhou Lu, and Wanying Yun. Active sparse polynomial chaos expansion for system reliability analysis. *Reliability Engineering & System Safety*, page 107025, 2020.

[92] Kai Cheng and Zhenzhou Lu. Adaptive bayesian support vector regression model for structural reliability analysis. *Reliability Engineering & System Safety*, 206:107286, 1920.

[93] C Lataniotis, S Marelli, and B Sudret. Uqlab user manual–the input module. *Chair of Risk, Safety and Uncertainty Quantification, ETH Zurich, Zurich, Switzerland, Report No. UQLab-V1*, pages 2–102, 2015.

[94] S Marelli, R Schöbi, and B Sudret. Uqlab user manual–structural reliability (rare event estimation). *Structural Reliability, Report UQLab-V0*, pages 9–107, 2016.

[95] Luc Schueremans and Dionys Van Gemert. Benefit of splines and neural networks in simulation based structural reliability analysis. *Structural safety*, 27(3):246–261, 2005.

[96] Junjie Wang, Tao Fu, and Yuanfeng Bao. Vessel-bridge collision risk analysis based on structural reliability theory. *Journal of Asian Architecture and Building Engineering*, 8(2):539–545, 2009.

[97] Yan-Gang Zhao, Xuan-Yi Zhang, and Zhao-Hui Lu. Complete monotonic expression of the fourth-moment normal transformation for structural reliability. *Computers & Structures*, 196:186–199, 2018.

[98] Chen Jiang, Haobo Qiu, Zan Yang, Liming Chen, Liang Gao, and Peigen Li. A general failure-pursuing sampling framework for surrogate-based reliability analysis. *Reliability Engineering & System Safety*, 183:47–59, 2019.

[99] Ning-Cong Xiao, Ming J Zuo, and Chengning Zhou. A new adaptive sequential sampling method to construct surrogate models for efficient reliability analysis. *Reliability Engineering & System Safety*, 169:330–338, 2018.